Structure and function of the EDEM:PDI ERAD checkpoint complex

Charlie J. Hitchman[1,2,11*], Andrea Lia[1,3], Gabriela N. Chiritoiu[4], Cristian V A Munteanu[4], Juan Ortigosa[5,6], Simona Ghenea[4], Christos Savva[1], Ikuo Wada[7], Maria De Benedictis[3], Gabor Tax[1], Yusupha Bayo[8,9], Irene Crescioli[8], Dominic L. Alonzi[10], Andrew Quigley[2], Carlos P. Modenutti[5,6], Stefana Petrescu[4], Angelo Santino[3*], Bibek Gooptu[1,2,11*], Pietro Roversi[1,8*]

[1]Leicester Institute of Chemical and Structural Biology and Department of Molecular and Cell Biology, University of Leicester, Henry Wellcome Building, Lancaster Road, Leicester, LE1 7HR, United Kingdom.
[2]Membrane Protein Laboratory, Diamond Light Source Ltd., Research Complex at Harwell (RCaH), Harwell Science and Innovation Campus, Didcot, OX11 0DE, United Kingdom.
[3]Institute of Sciences of Food Production, C.N.R. Unit of Lecce, via Monteroni, Lecce, I-73100, Italy.
[4]Department of Molecular Cell Biology, Institute of Biochemistry, Splaiul Independentei 296, Bucharest, 060031, Romania.
[5]Departamento de Química Biológica, Facultad de Ciencias Exactas y Naturales, Universidad de Buenos Aires, Ciudad Universitaria, Pab. II, Buenos Aires, CE1428EHA, Argentina.
[6]Instituto de Química Biológica de la Facultad de Ciencias Exactas y Naturales (IQUIBICEN) CONICET, Ciudad Universitaria, Pab. II, Buenos Aires, CE1428EHA, Argentina.
[7]Department of Cell Sciences, Institute of Biomedical Sciences, Fukushima Medical University School of Medicine, Fukushima, 960-1295, Japan.
[8]Institute of Sciences of Food Production, IBBA-CNR Unit of Milano, via Bassini 15, Milano, I-20133, Italy.
[9]Department of Biosciences, University of Milano, via Celoria 26, Milano, I-20133, Italy.

[10]Centre for Teaching and Learning, University of Oxford, Littlegate House, 16-17 St Ebbe's Street, Oxford, OX1 1PT, United Kingdom.
[11]Department of Respiratory Sciences, University of Leicester, Glenfield Hospital, Leicester, LE3 9QP, United Kingdom.

*Corresponding author(s). E-mail(s): angelo.santino@ispa.cnr.it; bg129@leicester.ac.uk; pietro.roversi@cnr.it;

Abstract

The ERAD glycoprotein misfolding checkpoint complex de-mannosylates misfolded glycoproteins, targeting them for retrotranslocation, ubiquitination, and proteasomal degradation. The checkpoint complex is a heterodimer comprising an Endoplasmic Reticulum Degradation Enhancing Mannosidase (EDEM) and a Protein Disulfide Isomerase (PDI). We determined Cryo-EM structures of the *Chaetomium thermophilum, (Ct) Ct*EDEM:*Ct*PDI heterodimer and its complex with a classic ERAD substrate, the $\text{Null}_{\text{HongKong}}$ variant of $\boldsymbol{\alpha}$1-antitrypsin (A1AT-NHK). The *Ct*EDEM:*Ct*PDI structure shows the EDEM catalytic domain nested within the PDI arc-shaped thioredoxin domains. In the complex with the client, A1AT-NHK contacts a hydrophobic surface in the EDEM C-terminal flexible domains. Redox chemistry between EDEM and PDI disulfide bonds yields an oxidized, demannosylation-competent EDEM and a reduced PDI, enabling the latter to act as the ERAD reductase in facilitating client retrotranslocation.

Keywords: ERAD, EDEM, PDI, CryoEM, A1AT-NHK

Introduction

The tangled mess that forms when headphone wires are stuffed into a pocket is a familiar, everyday example of entropy at work on objects with an excess of degrees of freedom. Freshly translated glycopolypeptides trying to fold in the endoplasmic reticulum (ER) of eukaryotic cells also have many degrees of freedom, and although they face much stricter folding controls than headphone wires — they, too, can end up in a tangled mess. Even worse: unlike headphone wires, which are topologically linear, glycoproteins often include disulfide bonds; when native cysteine pairings fail to form, a glycoprotein can adopt a nonlinear topology and become terminally misfolded.

Terminally misfolded glycoproteins are degraded by ER-associated degradation (ERAD [1–6]). ERAD of pathogenic mutant glycoproteins relieves ER stress and alleviates acute proteostatic challenges, although it underpins pathogenic loss-of-function phenotypes [7]. When glycoprotein misfolding within the ER overwhelms ER degradation capacity, the ER stress response is triggered [8]. Persistent misfolded proteins

not processed by ERAD are prone to toxic aggregation [9]. Chronic ER stress is a major mediator of chronic disease [10, 11].

ERAD detection of terminal glycoprotein misfolding is effected by ERAD checkpoint complexes [12], each of which comprises an ERAD enhancing mannosidase (EDEM) and a Protein Disulfide Isomerase (PDI). EDEM activity flags a terminally misfolded glycoprotein for degradation, by selective N-linked glycan demannosylation [13–16]. Once an EDEM has removed this mannose from the C branch of an N-glycan, the de-mannosylated glycoprotein proceeds to ERAD [16, 17] via selective recruitment by either the OS-9/Yos9/EBS6OS-9 or XTP3-B lectin, both of which are associated with the ERAD retrotranslocon [16, 18]. Through the latter, each EDEM-demannosylated glycoprotein is exported to the cytoplasm, where it is ubiquitinated and eventually digested by a proteasome [4, 5]. The molecular details underpinning initial recognition of misfolded glycoprotein recognition by ERAD checkpoint complexes are not known.

The first misfolded glycoprotein ERAD checkpoint was described in *Saccharomyces cerevisiae* as the disulfide-bonded HTM1P:PDI1P heterodimer [13, 19–21]. The heterodimeric nature of the ERAD misfolding checkpoint complex is functionally conserved across eukaryotes: each known EDEMs covalently interacts (via one or more disulfide bridges) with its own specific protein disulfide isomerase [13, 15, 19, 21–29]. In particular, three mammalian EDEM:PDI complexes have been described [30–33]: EDEM1:ERdj5 [22, 23, 26, 28, 34]; EDEM2:TXNDC11 [15, 24, 28]; and EDEM3:ERp46 [27, 29]. Despite the centrality of glycoprotein degradation to ER proteostasis [12, 35–37], the molecular determinants of misfolded glycoprotein recognition and de-mannosylation by the ERAD EDEM:PDI checkpoint complexes remain elusive.

We report here the first Cryo-EM structure of an EDEM:PDI complex, from the thermophilic yeast *Chaetomium thermophilum* (*Ct*). The *Ct*EDEM:*Ct*PDI structure provides the structural basis for branch C glycan specificity in EDEMs, and further shows EDEM and PDI are covalently linked by two disulfide bonds, each linking a free Cys on the EDEM with the first Cys of one of the PDI CXXC redox motifs. A low resolution Cryo-EM reconstruction of the *Ct*EDEM:*Ct*PDI complex with a classic ERAD substrate, the $\text{Null}_{\text{HongKong}}$ variant of α1-antitrypsin (A1AT-NHK) suggests that the mobile EDEM C-terminal domains are involved in the recognition of this terminally misfolded client, likely through interaction with exposed hydrophobic surfaces. In addition, biochemical studies with *Ct* and a human PDI indicate redox chemistry is essential for substrate recognition and activating EDEM, as well as in complex formation.

Results

Metazoan EDEM1s and EDEM3s evolved earlier than EDEM2s

All EDEMs include a domain belonging to the Glycosyl Hydrolase 47 (GH47) α-1,2-mannosidase family of enzymes. As well as the catalytic domains of EDEMs, the GH47 fold family also comprises ER Man I and other Golgi α-mannosidases [38][1].

[1] The Golgi endo-α-1,2-mannosidase (MANEA) which cleaves the A branch of the N-linked glycan belongs to a different fold family [39]

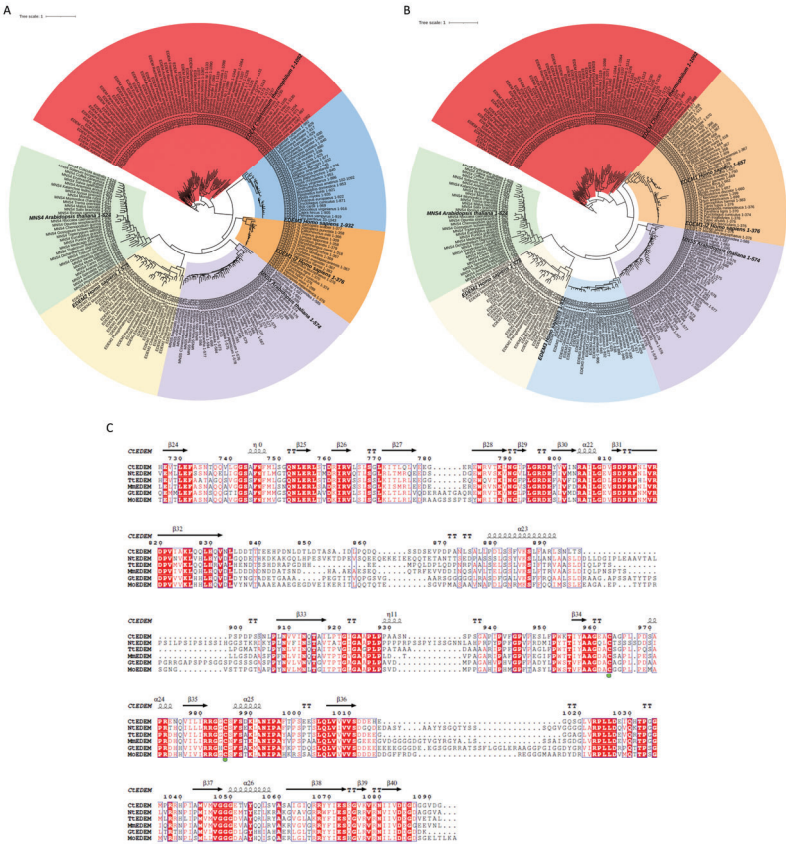

Fig. 1 EDEM phylogeny and C-terminal fungal EDEM domains A: Structure-based EDEMs phylogenetic tree. **B**: Sequence-based EDEMs phylogenetic tree. **C**: alignment of sequences of C-terminal intermediate domain (IMD) and protease-associated domain (PAD) tandems of fungal EDEMs. The Cys residues in the conserved disulfide bond at *Ct*EDEM Cys963:Cys985 are labelled with two green dots. *Ct*EDEM: *Chaetomium thermophilum*, Uniprot G0SCX7 · G0SCX7_CHATD; *Nt*EDEM: α-1,2-Mannosidase *Neurospora tetrasperma*, Uniprot F8N2I2 · F8N2I2_NEUT8; *Tt*EDEM: α-1,2-Mannosidase *Thermothielavioides terrestris*, Uniprot A0A3S4EST0 · A0A3S4EST0_9PEZI; *Mm*EDEM: α-1,2-Mannosidase *Madurella mycetomatis*, Uniprot A0A175VNQ1 · A0A175VNQ1_9PEZI; *Gt*EDEM: α-1,2-Mannosidase *Gaeumannomyces tritici*, Uniprot J3NGG5 · J3NGG5_GAET3; *Mo*EDEM: α-1,2-Mannosidase *Magnaporthe oryzae*, Uniprot G4NB03 · G4NB03_MAGO7.

In unicellular eukaryotes, only one EDEM gene is present [40]; plants have two genes annotated as EDEMs (MNS4 and MNS5) [41]; metazoans have three [42]. To elucidate the evolutionary relationships between EDEM proteins, we deployed structure-based and sequence-based phylogeny [43, 44], analyzing unicellular eukaryotic EDEMs, plant MNS4s and MNS5s, and metazoan *Hs*EDEM1/2/3s, with the initial sequence sets and homology models (Supplementary Figure S1) taken from the `AlphaFold Clusters` repository (https://cluster.foldseek.com/, [45]).

Figures 1A and B illustrate the EDEMs phylogenetic tree coming from structure-based and sequence-based phylogenesis respectively [43, 44]. Using the former approach, six branches emerge from the analysis, differing in sequence regions outside the GH47 domain:

1. unicellular eukaryotic EDEMs (red branch in Figure 1A): these proteins feature an N-terminal membrane associated region, a GH47 domain followed by a linker region, and two distinct C-terminal domains, which we call Intermediate Domain (IMD) and protease associated domain (PAD) - in keeping with the nomenclature established for mammalian EDEM3 in [29]. Figure 1C illustrates the alignment of the IMD+PAD part of sequence of a few fungal EDEMs;
2. metazoan EDEM3s (blue branch in Figure 1A): these proteins are the closest orthologues to the unicellular EDEMs and also feature the linker region and the two C-terminal domains - but lack an obvious N-terminal membrane-associated region [46];
3. metazoan EDEM1s (isoform 2[2]), orange branch in Figure 1A): the canonical EDEM1 isoform 2 lacks an N-terminal unstructured region [46], and have a ∼50-80 residue extension after the GH47 domain;
4. plant MNS5s (violet branch in Figure 1A) are similar to metazoan EDEM1s but have no membrane-associated N-terminal helix;
5. metazoan EDEM2s (yellow branch in Figure 1A) also feature a GH47 domain with a C-terminal extension;
6. plant MNS4s (green branch in Figure 1A) appear to be closest to metazoan EDEM2s and have an N-terminal membrane-associated region [46].

   Sequence-based methods produce similar results, but EDEM1s (orange branch in Figure 1B) look evolutionarily closer to unicellular eukaryotic EDEMs than EDEM3s (blue branch in Figure 1B).

The predicted intrinsically disordered region at the C-terminal (IDR(C)) of EDEM1 [26] that extends from the GH47 domain is essential for its interaction with thioredoxin domain (TRX4) of its partner PDI, ERdj5 [34]. Our analysis identified a similar region in EDEM1, EDEM2 and their orthologues. In EDEM3 and its orthologues the GH47 tail is longer (about ∼80 residues) and it is followed by one or two C-terminal domains. For this reason, the EDM3 GH47 tail is often referred to as the EDEM3 linker region. The EDEM3 tail (*aka* linker region) also contains the conserved Cys (CysA) capable of disulfide bonding to a PDI redox motif to stabilize the EDEM:PDI complex [15, 19, 26]. Moreover, the longer EDEM3 tails contain a second unpaired cysteine residue (CysB), located in the sequence between CysA and the C-terminal domains (Supplementary Figure S2), that may also form an inter-molecular disulfide bond with the partner PDI [19, 27].

[2]The unstructured N-terminal region of the EDEM1 isoform 1 aligns well with the N-terminal section of fungal EDEMs - but the protein lacks the extra C-terminal domains. Structure-based and sequence-based phylogeny therefore give different results and EDEM isoform 1 sequences have been omitted from the structure-based analysis.

Oxidation of a conserved disulfide bond in the EDEM GH47 domain is necessary for function and requires PDI association

Structure-based sequence alignment [47] of the GH47 domain and linker region of unicellular EDEMs and metazoan EDEM3s, based on the available `AlphaFold` models [48] of the same proteins (Supplementary Figures S1 and S2) has revealed that EDEMs share a conserved, surface-exposed intra-molecular disulfide, *e.g.* *Ct*EDEM C99-C558; *Hs*EDEM3 C82-C441; *Mm*EDEM3 83-442; *Sc*HTM1P C65-C445; *Hs*EDEM1 C160-C529; *Hs*EDEM2 C65-C408 (Supplementary Figure S2). This disulfide bond is very close to the GH47 domain glycan binding site (see Figure 2C) and its correct oxidation is likely necessary for EDEM competency/function. Interestingly, in the presence of excess glutathione *in vitro*, which reduces the EDEM3 disulfide bond, EDEM3 enzymatic activity can be restored by its partner PDI ERp46, suggesting that this intramolecular SS bond is in mutual redox dependency with one of the PDI CXXC motifs and/or the intermolecular disulfide(s) mediating the covalent EDEM:PDI association [27]. Similar data suggest the same for *Sc*HTM1P and *Hs*EDEM2 [15, 19]. It is tempting to speculate that all ERAD mannosidases need SS-bond mediated association with their partner PDI and the oxidation of their intramolecular conserved SS bond to be active [15, 19, 27].

Unpaired Cys residue(s) in the EDEM GH47 tails

As mentioned above, a stretch of sequence follows the GH47 domain in all EDEMs: in EDEM1, EDEM2 and their orthologues, this GH47 tail is ∼50-residue long and it ends in the protein C-terminus, while in EDEM3 and its orthologues it is ∼80-residue long and followed by one or two C-terminal domains. In EDEM1, this stretch is referred to as the C-terminal intrinsically disordered region (IDR(C)) because sequence analysis suggests an absence of secondary structure: together with another intrinsically disordered region, at the N-terminal (IDR(N)) of EDEM1, the IDR(C) is essential for its interaction with the ERdj5 partner protein PDI [26]. The latter interacts with EDEM1 using its fourth thioredoxin domain (TRX4) domain [34].

In all EDEMs, the GH47 tail contains a conserved Cys residue (termed Cys_A), *e.g.* *Hs*EDEM1 Cys629 (*Mm*EDEM1 Cys624); *Hs*EDEM2 Cys558; *Hs*EDEM3 Cys528 (*Mm*EDEM3 Cys529); *Sc*HTM1P Cys579 and *Ct*EDEM Cys647. Biochemical experiments show that Cys_A can establish an EDEM:PDI intermolecular disulfide bond with the first Cys of one of the redox-active CXXC motifs on the PDI. Indeed, in the *Sc*HTM1P:PDI1P Cryo-EM structure, *Sc*HTM1P Cys579 is within disulfide bond distance from Cys406 of the ^{406}CXXC^{409} motif of the first TRX domain (TRX1) of *Sc*PDI1P [49].

Homology modelling of the human EDEM:PDI complexes and biochemical data on the same proteins also suggest an equivalent inter-molecular disulfide bridge involving Cys_A and one of the redox-active CXXC motifs on the PDI in each of the three ERAD checkpoint EDEM:PDI complexes. In the *Hs*EDEM1:ERDJ5 complex, Cys158 of the ^{158}CXXC^{161} motif in the first TRX domain (TRX1) of *Hs*ERDJ5 can form a disulfide with *Hs*EDEM1 Cys629 [26]; in the *Hs*EDEM2:TXNDC11 complex, the disulfide bridge would be between Cys692 in the TRX5 domain of *Hs*TXNDC11 [15]

and *Hs*EDEM2 Cys558; and in the EDEM3:ERp46 complex, between Cys217 in the TRX1 domain of *Hs*ERp46 [15] and *Hs*EDEM3 Cys528.

As already mentioned, the linker regions of unicellular EDEMs and EDEM3s are longer than the stretch following GH47 domains in EDEM1s and EDEM2s. In that linker, each EDEM3 sequence has a second unpaired cysteine residue located downstream from Cys_A and preceding the C-terminal domains (Supplementary Figure S2). This second Cys residue, only present in unicellular EDEMs and metazoan EDEM3 orthologues, is termed Cys_B (for example *Ct*EDEM C719, *Mm*EDEM3 C558 and *Sc*HTM1P C644,Supplementary Figure S2). Biochemical data suggest that *Hs*EDEM3 and *Sc*HTM1P can also form an inter-molecular disulfide bond with the partner PDI [19, 27]. The same is true for Cys_A in *Hs*EDEM2, which is also essential for EDEM2-mediated degradation of an EDEM2 substrate: it forms an intermolecular disulfide bond with its PDI, *Hs*TXNDC11 [15, 24].

The *Chaetomium thermophilum* EDEM:PDI heterodimer functions as an ERAD checkpoint in plants and human cells

We decided to work with ERAD checkpoint proteins from the thermophilic yeast *Chaetomium thermophilum* (*Ct*) in order to profit from their enhanced protein stability [50]. A search in the *Ct* genome using the protein sequence of *Saccharomyces cerevisiae* HTM1P yielded Uniprot entry https://www.uniprot.org/uniprot/G0SCX7 (hereinafter *Ct*EDEM), annotated as α-1,2-mannosidase; a search in the same genome using the protein sequence of *Sc*PDI1P yielded Uniprot entry https://www.uniprot.org/uniprot/G0SGS2 (hereinafter *Ct*PDI), annotated as a protein disulfide isomerase. In agreement with the phylogenetic analysis, the same Uniprot entries were hit by searching the *Ct* genome with the sequences of *Hs*EDEM3 [33] and its partner PDI, *Hs*ERp46 [27].

First, we set out to assay ERAD mannosidase activity of *Ct*EDEM. We did so *in planta*, using a complementation transfection assay in *Arabidopsis thaliana*. This is based upon the dwarf phenotype associated with expression of a brassinosteroid receptor (BRI1) misfolding mutant (bri1-5). When the plant EDEMs MNS4 and 5 are also deleted (*At mns4-1 mns5-1 bri1-5*) a wild-type growth phenotype is rescued [41, 51]. *Ct*EDEM transfection resulted in functional re-complementation of EDEM, commitment of the BRI1 variant to ERAD and restoration of a dwarf phenotype (Supplementary Figure S3). Use of fluorescent-tagged *Ct*EDEM constructs confirmed its localization to the plant ER (Supplementary Figure S4).

Secondly, we assayed *Ct*EDEM ERAD mannosidase activity in human cells. HEK293T EDEM3 KO cells were co-transfected with *Ct*EDEM, *Ct*PDI or both, together with a canonical ERAD substrate, the $\text{Null}_{\text{HongKong}}$ variant of α1-antitrypsin (A1AT-NHK, Supplementary Figures S3B, C and D). Following cleavage of the secretory signal peptide upon entry to the ER, A1AT retains a single cysteine residue (Cys 232) which can either form an inter-molecular disulfide bond with human ERAD checkpoint complexes, or with itself, leading to A1AT dimers. Disulfide bonding of A1AT variants results in prolonged retention within the ER [52]. When *Ct*PDI was overexpressed in the absence of *Ct*EDEM the A1AT-NHK dimer:monomer equilibrium shifted towards the monomer (Supplementary Figure S3C). In cells transfected with

*Ct*EDEM (both alone and with *Ct*PDI) degradation of A1AT-NHK was enhanced, with reduction in both dimeric and monomeric protein levels (Supplementary Figures S3B and D).

Cryo-EM structure of *Ct*EDEM:*Ct*PDI

The *Ct*EDEM:*Ct*PDI ERAD checkpoint complex was expressed and purified from HEK293F cells using affinity and size exclusion chromatography, and Cryo-EM grids were prepared with a *Ct*EDEM:*Ct*PDI sample eluted from a Micro-SEC column (Supplementary Figures S5 and S6). Cryo-EM data collection yielded a total of 11,208 micrographs from which a total of 6,579,255 particles were picked and selected by rounds of 2D classification. After *ab initio* reconstruction and three rounds of decoy classification using cryoSPARC™ with heterogenous refinement, 3D classification on a subset of 624,939 particles gave 4 3D classes for the complex. The largest volume pertains to a class with approximate dimensions 120x90x70 Å(Supplementary Figure S7A), which has strong density for all but the C-terminal domains of *Ct*EDEM. Density was also visible for the N-terminal GFP tag and was subsequently removed by particle subtraction. The local resolution of this Cryo-EM reconstruction varies between 2.7 Å in the core of the GH47 *Ct*EDEM domain, to 2.8-3.2 Å in the four TRX domains of the *Ct*PDI to 3.8-5.5 Å in the C-terminal domains of *Ct*EDEM (Supplementary Figure S8).

`AlphaFold` domain models were initially docked into the Cryo-EM map by phased molecular replacement using `CCP4-Molrep` [53], followed by iterative model building and refinement. The EDEM catalytic domain nestles inside the curved arc formed by the PDI thioredoxin (TRX) domains TRX1, TRX3 and TRX4 (yellow, brick-red and red domains in Figures 2A and B). The exposed *Ct*EDEM Leu656 forms an intermolecular hydrophobic contact with the *Ct*PDI surface pocket formed by Tyr238, Tyr250 and His290, equivalently to what observed in the *Saccharomyces cerevisiae* *Sc*HTM1P:*Sc*PDI1P orthologous complex structure (where *Sc*HTM1P Trp592 and Tyr593 interacts with *Sc*PDI1P Phe249, Tyr261 and His301) [49].

The first three TRX domains of *Ct*PDI adopt the threefoil/cloverleaf structure typical of the N-terminal portion of most PDIs (yellow, orange and brick-red domains at the top of Figures 2A and B), with TRX2 jutting out and not contacting *Ct*EDEM at all. The IMD and PAD [29] (*Ct*EDEM residues 726-821, 1069-1092 and residues 822-1068, respectively) project out from the GH47 domain (Figures 2A and B). *Ct*EDEM residues 1069-1083 following the PAD, contribute a β strand to the IMD β sandwich, *i.e.* the PAD is an insertion in the sequence encoding the IMD. A 56-residue stretch of *Ct*EDEM PAD sequence (845-900) and the C-termini of both proteins (*Ct*EDEM 1084-1093 and *Ct*PDI 484-515) could not be traced.

The refined model and Cryo-EM map were deposited in the Protein Databank (PDB) and in the Electron Microscopy Data Bank (EMDB), with deposition IDs 8PKO and EMD-17749, respectively (deposition date: 2023-06-27). In the period between the deposition of the structure and its release, *Ct*EDEM:*Ct*PDI was contributed to the list of CASP-15 protein prediction targets (CASP-15 Target H1157 https://predictioncenter.org/casp15/target.cgi?id=116&view=all: a brief

description of how the predictors did on this target was published in [54]. During the preparation of this manuscript, a paper describing the Cryo-EM structure of the *Saccharomyces cerevisiae* EDEM:PDI heterodimer (*Sc*HTM1P :*Sc*PDI1P) was published [49] and deposited (EMDB and PDB accession codes EMD-60365 and 8ZPW, respectively). The *Sc*HTM1P :*Sc*PDI1P structure has equivalent quaternary structure to *Ct*EDEM:*Ct*PDI. The GH47 domains are very similar: overall *Sc*HTM1P $_{\mathrm{GH47}}$:*Ct*EDEM$_{\mathrm{GH47}}$ rmsd$_{\mathrm{C}\alpha}$ over 397 residues is 1.0 Å. The *Sc*PDI1P :*Ct*PDI rmsd$_{\mathrm{C}\alpha}$ over 402 residues is 3.2 Å.

The *Ct*EDEM mannosidase

As predicted by the `AlphaFold` model, the *Ct*EDEM the catalytic domain of the mannosidase (*Ct*EDEM residues 64-615) has the classic GH47 (α/α)7-barrel fold, with the active site at the base of the barrel, plugged by a β-hairpin at the C-terminus (*Ct*EDEM residues 602-615, [55, 56], (Figures 2A and B). The *Ct*EDEM active site features the canonical GH47 conserved acidic catalytic residues E191, D370, E522, and the conserved T608 coordinating the Ca^{++} ion with its main chain carbonyl and $O_{\gamma 1}$ atom (see Figures 2C and D and blue triangles in Supplementary Figure S2)[3].

In other deposited apo GH47 structures, the octahedral coordination of the catalytic divalent ion is usually completed by six water molecules [55, 56]. Substrate binding usually displaces two of the water molecules through coordination with the O2' and O3' hydroxyls of the terminal α1,2-mannose residue within the catalytic -1 subsite. In our Cryo-EM map there is density for a ligand bound in the active site consistent the same coordination geometry [38] (Figure 2C)[4].

The GH47 domain is followed by a 120-AA long EDEM-specific portion of structure (*Ct*EDEM residues 616-725) which mediates most of the contacts to the PDI. The first stretch of this portion (*Ct*EDEM residues 616-651, coloured cyan in Figures 2A,B) is an L-shaped linker which starts after the GH47 C-terminal hairpin, sits over *Ct*EDEM helices α9/α10 and α13/α14 and wraps over the surface of the PDI TRX4 domain, eventually running parallel to the PDI TRX3-TRX4 linker (*Ct*PDI residues 616-655). This L-shaped linker contains the conserved *Ct*EDEM Cys647 that forms the inter-molecular SS bond to *Ct*PDI Cys385 of the PDI-TRX4 CXXC redox motif (the disulfide bond is labelled "SS1" in Figures 2A and B and its close-up view is shown in Supplementary Figure S9B). This disulfide bond is structurally and functionally equivalent to the one between *Hs*EDEM2 Cys_A (Cys) and Cys692 in the TRX5 domain of its PDI, *Hs*TXNDC11, which is necessary for function [15, 24].

After the L-shaped linker, a helical linker sub-domain (*Ct*EDEM residues 656-713, cyan in Figures 2A and B) nestles between helices α14/α15 of the GH47 domain and the TRX1 domain of the PDI. A `Dali` search [60] with the linker sub-domain does not

[3] *Ct*EDEM E191 is the residue corresponding to *Mm*EDEM3 E147, *Hs*EDEM1 E225, *Mm*EDEM1 E220 and *Hs*EDEM2 E117 each of which when mutated to Q abrogate mannosidase activity respectively [14, 33, 57, 58]. *Ct*EDEM D370 is the residue corresponding to *Sc*HTM1 D279 which when mutated to N abrogates mannosidase activity [13]. *Ct*EDEM E522 is the residue corresponding to *At*MNS4 E376 and *At*MNS5 E388 which when mutated to N abrogate mannosidase activity [41].

[4] The ligand pose is similar to the one of D-Mannose analogues 1-deoxymannojirimycin and kifunensine (PDB IDs 1FO2 and 1FO3) [55] and of the -1 mannose ring of the thio-disaccharide substrate analogue co-crystallised in the active site of the GH47 domain of ER Man IB (PDB ID 5KK7 [59]).

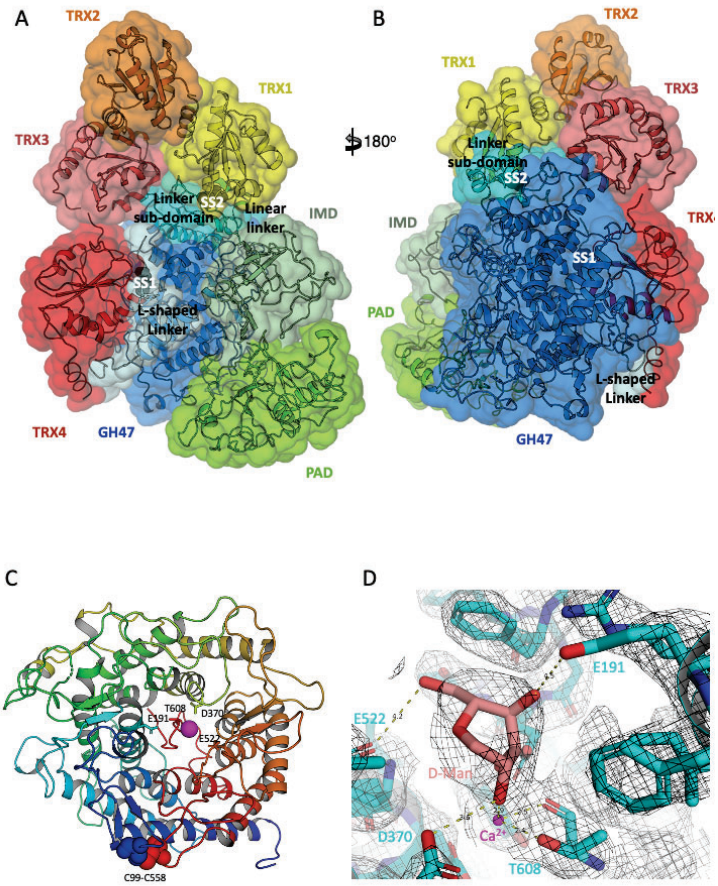

Fig. 2 The Cryo-EM *Ct*EDEM:*Ct*PDI ERAD checkpoint structure. A,B: Two views of the *Ct*EDEM:*Ct*PDI ERAD checkpoint structure in cartoon and transparent surface representation. Left-hand and right-hand side view are related by a rotation of 180 ° around the vertical axis. *Ct*EDEM domains: GH47 catalytic domain (56-615, blue); L-shaped linker, linker domain and linear linker (616-655, pale cyan; 656-713, cyan; and 714-725, green cyan); IMD (726-821 and 1069-1092, pale green); PAD (822-1068, green). *Ct*PDI domains: TRX1 (18-128, dark yellow); TRX2 (129-228, orange); TRX3 (229-342, brick red); TRX4 (343-484, red). The Ca^{++} ion is a magenta sphere. The two inter-chain disulfide bonds are represented in spheres and labelled SS1 (*Ct*EDEM Cys647:*Ct*PDI Cys385) and SS2 (*Ct*EDEM Cys719:*Ct*PDI Cys50); **C**: cartoon representation of the *Ct*EDEM GH47 catalytic domain, painted blue to red from N- to C-terminus. The side chains of the catalytic site conserved residues E191, D370, E522 and T608 are in sticks representation. The conserved *Ct*EDEM C99-C558 intramolecular disulfide bond is in spheres representation. **D**: Cryo-EM map in the *Ct*EDEM active site, represented as a mesh at level 10.0σ. O atoms: red; N atoms: blue; protein C atoms: cyan; D-mannose C atoms: salmon. The distances between the D-mannose/Ca^{++} ion and their coordinating residues are represented as dashed yellow lines. Figure made in `PyMOL`.

detect any structural homology with any of the protein domains in the Protein Databank. This sub-domain is followed by a short linear linkage motif (*Ct*EDEM residues 714-725) which contains the conserved *Ct*EDEM Cys719 forming the inter-molecular SS bond to *Ct*PDI Cys50 of the PDI-TRX1 CXXC redox motif. This disulfide bond is labelled "SS2" in Figures 2A and B and a close-up view shown in Figure S9A.

As already mentioned, the IMD and PAD are topologically intertwined (Figure 2C). The PAD is encoded by a stretch of sequence between the majority of the IMD and the C-terminal 24 residues of the *Ct*EDEM protein. The latter form a two-stranded β sheet that completes the β sandwich fold of the IMD. `AlphaFold` correctly predicted this topological feature but did not predict correctly the relative orientation of the IMD-PAD tandem with respect to the GH47 domain. The main IMD:GH47 contact is formed by the hairpin *Ct*EDEM residues 778-782 (Figure 2C), nestling in a shallow surface pocket of the GH47 domain (*Ct*EDEM residues 437-460).

The observed *Ct*EDEM:*Ct*PDI interface rationalises the loss of function of mutants of *Ct*EDEM orthologues. *Sc*HTM1P mutants D607A, E627A, W636A, F632L and Y633S abrogate the association with *Sc*PDI1P [19, 61]; the G343E mutant of the *Arabidopsis thaliana* plant EDEM orthologue MNS5 abrogates ERAD mannosidase function. The equivalent residues in *Ct*EDEM R672, H669, L712, L703, Y704 and G477 respectively, all map to the interface between *Ct*EDEM and *Ct*PDI in our structure (Supplementary Figure S10). The loss of function associated with the deletion of the 4 C-terminal residues of *Sc*HTM1P [19] is also explained by the damage inflicted to the fold of the IMD domain.

*Ct*EDEM glycan-specificity is associated with alterations at the entrance of the mannosidase active site

In mammals, there are seven GH47 members, including ER α1,2-mannosidase I (ERManI); the three Golgi α1,2-mannosidases GMIA, GMIB, and GMIC [59]; and the three ER degradation-enhancing α-mannosidase-like (EDEM) proteins (EDEM1 [14, 26, 31, 62, 63], EDEM2 [64], and EDEM3 [33]), the ERAD misfolded glycoprotein checkpoints. The GH47 domains of these proteins share a common fold and differ in insertion loops. Five *Ct*EDEM regions (labelled "II" to "VI", residues (140-150), (165-180), (205-235), (280-300), and (390-420) respectively) are surface loop insertions only present in thermophilic EDEMs but not in other GH47 domains (Supplementary Figures S2 and S11). These regions are contiguous in space and form a surface which is specific to thermophilic EDEMs but not to other orthologues (Supplementary Figure 3).

Structures of GH47 α1,2-mannosidases have been determined in the absence and presence of inhibitors, substrate analogues and substrate glycans [55, 56, 59, 65]. In contrast to the highly conserved -1 and +1 subsites, the structures of the substrate-binding groove are distinct among the GH47 family members. These groove features are the main determinants for selectivity towards the cognate *N*-linked glycan branch that inserts in the active site [59, 65].

Region "I", *Ct*EDEM comprises residues 100-118 and is conserved across 600 sequences or so (Supplementary Figure S11) that are likely to be *Ct*EDEM close orthologues. In the structure, this region is a surface loop including an α helix (*Ct*EDEM

helix α2, residues 111-118, 3, hot pink) which is not present in the structures of ER Man IB and occupies the space where the first branching mannose of the N-glycan ("C" in Supplementary Figure S12) and the first mannose of the *N*-glycan A branch ("D" in Supplementary Figure S12) bind ER Man IB (PDB ID 5KIJ [59]) and Golgi α-Mannosidase IA (PDB ID 1DL2 [55]). The volume taken up by the *Ct*EDEM α helix in region "I" suggests that EDEMs bind the A branch of the *N*-linked glycan differently from ER Man IB and Golgi Man IA. In particular, at the position corresponding to *Ct*EDEM Val117, a methyl group is likely to be involved in contacting the "J" mannose in branch C (see Figure S12). This region's conformation depends on the formation of the conserved intramolecular disulfide bond, which only forms in presence of the partner PDI [15, 19, 27].

In the Cryo-EM map, *Ct*EDEM Cys303 appears modified covalently and was tentatively modelled as Cys-S-sulfonate [66] (this position is Thr or Ser in ER Man IB and Golgi α-Mannosidase IA, respectively). A key Arg residue (Arg273), conserved among the ER mannosidase IB subfamily of enzymes, was found to interact with several residues in their active site and to contribute to branch specificity [67]. The equivalent residue to Arg273 of ER Man1B in *Ct*EDEM is Gly368: in all EDEMs this residue is either Glycine or Serine (Supplementary Figure S2). As these are both smaller amino acids than Arg, this position may be a key determinant of glycan branch specificity in EDEMs vs. ER Man IB.

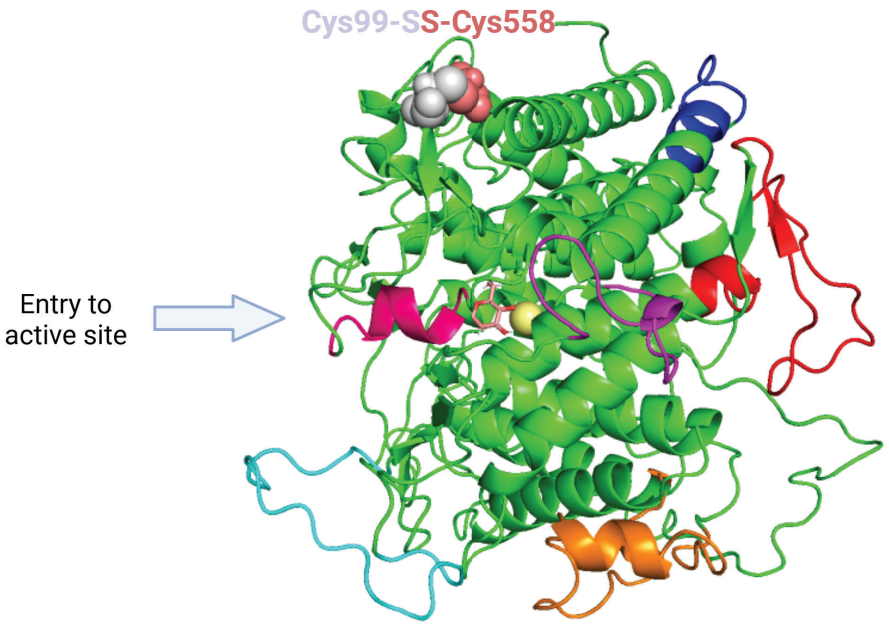

Fig. 3 *Ct*EDEM active site with short helix and loop insertions. Top view of the GH47 catalytic domain of *Ct*EDEM with short α helix and surface loop insertions highlighted. The short α helix, residues *Ct*EDEM 110-118 is highlighted in hot pink, the loop insertions of residues *Ct*EDEM 140-150, 165-180, 205-235, 280-300, and 390-420 are coloured dark blue, magenta, red, cyan, and orange respectively. These six regions correspond to I-VI in Figure S11. The Ca^{++} ion is represented as a sphere and coloured light yellow. The D-Mannose in the active site is coloured by atom (carbon = orange, oxygen = red). The conserved intramolecular disulphide bond is shown with Cys99 in light grey and Cys558 in salmon.

*Ct*EDEM:*Ct*PDI inter-domain conformational flexibility

3D variability analysis (3DVA) in cryoSPARC™ was utilised to investigate the flexibility of *Ct*EDEM:*Ct*PDI portions built in volumes with lower local resolution. 3DVA analysis of the particles within the dataset suggested three specific movements. The first involved the IMD and PAD (Figure 4i) and the second and third involved movement of the three-leaf clover PDI tail (Figure 4ii and 4iii). The first movement can be described as a twisting and pivoting of the IMD and PAD around the main axis of the particle and away from the active site face of the GH47 domain while the three-leaf clover and the GH47 domain remain relatively unperturbed (Supplementary Videos 1 and 2). The second movement involves a twisting of the TRX1-3 domains with respect to TRX4 and EDEM (Supplementary Video 4). Figure S13 shows EM maps obtained from particles sampling the endpoints of the third movement. The PDI three-leaf clover straightens (bends) with respect to the main body of the complex, so that the

particle toggles between a linear (Figure S13A-C, yellow map) and a bent conformation (Figure S13A-C, blue map). Supplementary Video 3, shows the three-leaf clover undergoing an angular change of approximately 15°. The observed conformational flexibility is highly consistent with biophysical studies of PDIs [68, 69].

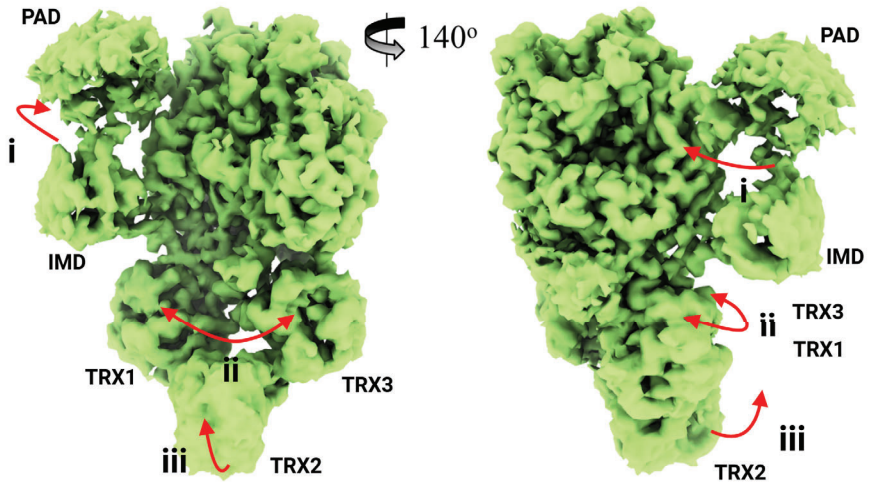

Fig. 4 *Ct*EDEM IMD-PAD and *Ct*PDI TRX1,2,3 domains exhibit a range of inter-domain conformations. 3D variability analysis in cryoSPARC displayed three principles ranges of motion: i) front-to-back and up-and-down action of the *Ct*EDEM IMD and PAD. ii) twisting movement of *Ct*PDI TRX1-3 domains. iii) flapping of the *Ct*PDI TRX2 domain.

*Ct*EDEM:*Ct*PDI surface hydrophobic patches localise to the flexible IMD+PAD and TRXL2 domains

The canonical function of the PDI:EDEM complex is to act as a checkpoint for ERAD, but the presence of the PDI is reminescent of the role of TRX domains in chaperone-promoted refolding [70, 71]. Chaperones often interact with exposed hydrophobic regions of misfolded proteins, limiting the risk of pathogenic aggregation and lowering energetic barriers to refolding pathways [72–74]. UGGT, the ER retention checkpoint, recognizes misfolded glycoproteins and delays ERAD targeting by substrate re-glucosylation [75]. In addition, UGGT may act as a re-folding chaperone [76, 77], forms a tight complex with the Sep15 thioredoxin [78], and its activity may be mediated by the ability of its thioredoxin-like (TRXL) domains to bind linear peptides [79, 80].

Inspired by the similarities between the UGGT:Sep15 ER retention checkpoint and the EDEM:PDI ERAD checkpoint, we set out to look for surface regions of the PDI:EDEM heterodimer with the potential to interact with exposed hydrophobic motifs of misfolded proteins. Non-polar surfaces were identified using the `protein-sol` server (https://protein-sol.manchester.ac.uk/ [81]).

Two hydrophobic regions were identified on the EDEM:PDI surface: the face of the *Ct*EDEM IMD-PAD arm to the side of the GH47 face at the centre of which the active site is found (*Ct*EDEM IMD residues 728-732, 745-749, 792-794; PAD residues 832-835, 906-912, 939-947); and the lower tip of the *Ct*PDI TRX2 domain (*Ct*PDI, Val133, Leu138, Val150 and Phe141). These regions are coloured green in Figure 5. The same IMD+PAD and TRX2 domains have been identified as highly flexible (previous section), making them prime candidates as mediators of recruitment of misfolded glycoprotein substrates to the enzyme.

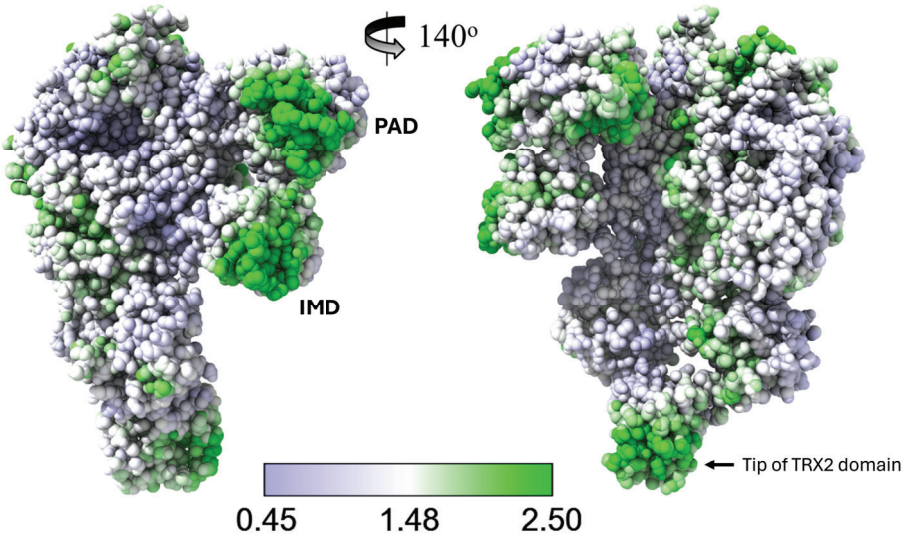

Fig. 5 *Ct*EDEM:*Ct*PDI surface hydrophobic patches localise to the flexible IMD+PAD and TRXL2 domains. Two views (related by a rotation of 140° around the vertical axis) of the *Ct*EDEM:*Ct*PDI heterodimer model are displayed in spheres representation and coloured by surface hydrophobicity, calculated as the ratio of non-polar to polar residues [81]. Hydrophilic regions are painted pale violet and hydrophobic regions are painted green, as indicated by the hydrophobicity scale bar.

EDEM:PDI substrate recognition and recruitment

*Ct*EDEM:*Ct*PDI interacts with NHK-A1AT substrate through hydrophobic interactions on the mobile IMD-PAD domain

Coexpression of *Ct*EDEM and *Ct*PDI in HEK293F cells was repeated with cotransfection of a plasmid containing the NHK variant of alpha-1 antitrypsin. A ternary complex of the three proteins was extracted from the cells (Figure S14) and studied by cryo-EM.

A dataset of 7773 movies was collected and processed as for the checkpoint apo-complex.(Figure S15). Two distinct populations of 2D classes were noticed, consistent with the heterodimer -/+ extra density, corresponding to the NHK substrate binding.

Initial reconstructions of the ternary complex particles were relatively low resolution but displayed clear density adjacent to the core heterodimer particle. A mask was generated to cover the heterodimer particle and used in a focused 3D classification. Four classes were generated and the best map and particles were taken forward for 3D refinement. The final EM map has an estimated global resolution of 9Å although the region of extra density is lower. However, the region of extra density is less resolved, consistent with highly disordered conformational behaviour.

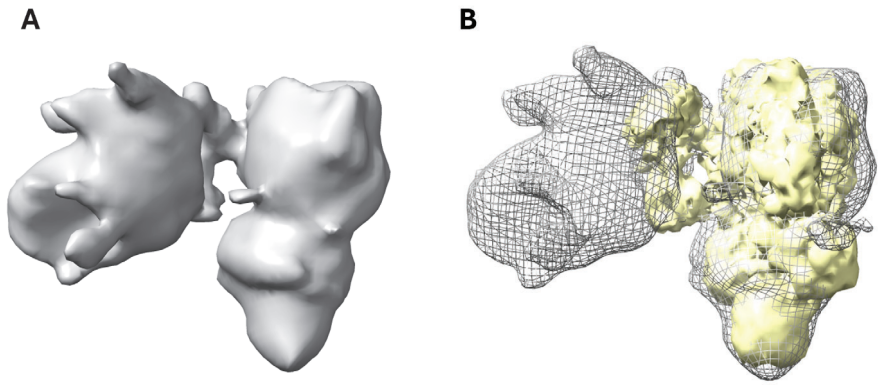

Fig. 6 Low resolution Cryo-EM maps of PDI:EDEM:NHK with fitted PDI:EDEM heterodimer map A. The Cryo-EM map of PDI:EDEM:NHK displayed in UCSF `ChimeraX` [82]. B. The map of PDI:EDEM:NHK in grey mesh with the PDI:EDEM heterodimer map fitted within in yellow.

Overlaying the EM map of the EDEM:PDI heterodimer onto the ternary complex map shows a close fit (Figure 6). Furthermore, the extra density adjacent to the core heterodimer particle in the ternary complex aligns with the location of the *Ct*EDEM C-terminal domains in the heterodimer. No gross change in the relative orientations of PDI and EDEM was apparent at this resolution. Extra density was visible adjacent to the PDI:EDEM density, likely representing the bound NHK substrate. The interface between NHK and PDI:EDEM localises to the mobile *Ct*EDEM IMD-PAD arm. This provides strong support for the hypothesis that the surface hydrophobic patch on this motif generically recruits misfolded substrates *in situ* analogous to recruitment in chaperones.The extra volume is larger than expected for *Ct*EDEM C-terminal domains and a single copy of NHK. This could be because of inherent interdomain mobility of the substrate relative to the checkpoint core, but a corresponding reduction in its average density is not observed. Alternatively NHK may bind this site in dimer and/or oligomeric states.

*Ct*EDEM:*Ct*PDI forms mixed disulfide bonds with NHK-A1AT

The N-terminal cysteines within the CXXC redox motifs in active sites of protein disulphide isomerases (CGHC in CtPDI) [83] can form disulphide bonds within the

same protein, or with cysteines in other proteins. In the EDEM:PDI heterodimer structure, these are formed with EDEM. When acting as chaperones, PDIs generally use these to interact with misfolded substrates, to facilitate re-folding, specifically via disulphide isomerisation [84]. PDI chaperone function proceeds via the C-terminal cysteine in the CXXC motif re-forming a disulphide bond with its N-terminal neighbour, thereby releasing the substrate. However, if the C-terminal cysteine is mutated to a redox-inactive residue with similar chemical and steric properties, *e.g.* alanine or serine, the substrate remains trapped in complex with PDI. CXXA or CXXS mutants of PDI are therefore known as trapping mutants [85]. We demonstrated that a Cys53Ser *Ct*PDI trapping mutant enhanced population of both PDI:EDEM covalent complexes and ternary complex states, indicating that PDI Cys53 can alternatively bind EDEM or substrate cysteines (Figure 7). Substrate binding at redox motifs will therefore inherently increase inter-domain flexibility.

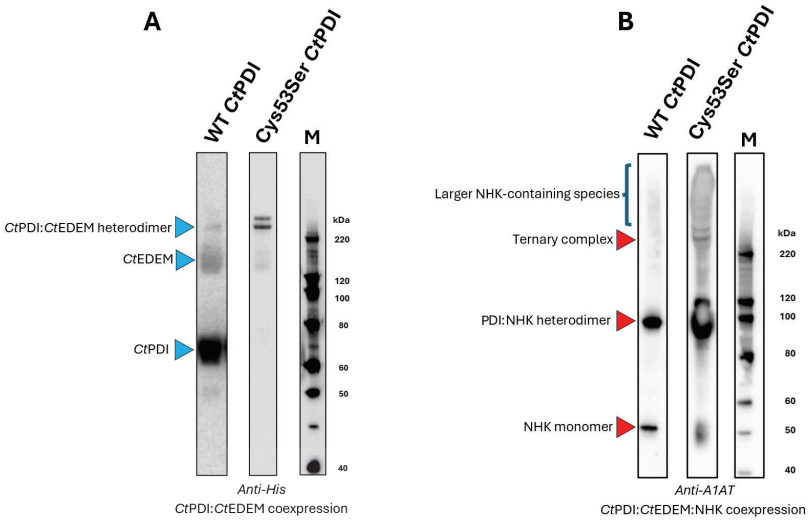

Fig. 7 Cys53Ser *Ct*PDI trapping mutant favours disulphide bond formation with *Ct*EDEM and NHK HEK293F cells were co-transfected *Ct*EDEM A1AT NHK, and either wild-type *Ct*PDI or Cys53Ser *Ct*PDI. Heterodimer or Ternary complexes were purified from the media by IMAC followed by SEC (see Section on Protein purification). Fractions collections from both SEC experiments were loaded in non-reduced (NR) conditions in 4-12% polyacrylamide gels, transferred on nitrocellulose membrane and probed with indicated antibodies: rabbit anti-α1 Antitrypsin (A1AT), mouse anti-His for detection of *Ct*PDI and *Ct*EDEM. A. Anti-His Western blot from *Ct*EDEM:*Ct*PDI (WT and mutant) heterodimer co-purification with a SEC fraction corresponding to the heterodimer peak. B. Anti-A1AT Western blot from ternary complex co-purification with a SEC fraction corresponding to the ternary complex peak. The identity of the 100 kDa band as *Ct*PDI:NHK heterodimer was confirmed by Western blot with anti-His. Full purification SDS-PAGE and Western blot results are shown in Supplementary figures S14 and S16.

SEC fractions corresponding to the ternary complex with A1AT-NHK substrate demonstrated an ensemble of such states. A1AT-NHK was observed in a non-covalently

associated state, covalently bound to *Ct*PDI, and in a ternary complex in which covalent bonds held all three proteins together. The presence of the *Ct*PDI Cys53Ser trapping mutation stabilized the covalent binding of A1AT-NHK to PDI relative to the non-covalently associated state. This finding supports ready reversibility of disulfide bonding behaviour between wild-type CtPDI Cys50 and substrate cysteines in the ternary complex.

Redox chemistry is essential for substrate recognition and mannosidase activity in human EDEM3

Building on our structural and functional characterization of the Chaetomium thermophilum EDEM:PDI complex and its interactions with the human A1AT-NHK mutant, we extended our analysis to the human orthologue, EDEM3:ERp46, to assess the conservation of these mechanisms in the mammalian ERAD pathway.

*Hs*ERp46 can form intermolecular disulfide bonds with peroxiredoxin 4 (PRXD4) using the first Cys of its CXXC redox motif in it middle domain, Cys217 [86, 87]. Evidence that *Hs*ERp46 forms a mixed disulfide bond with a client glycoprotein has also been obtained in the context of its refolding role, where it catalyses the reduction of non-native disulfides [88].

In order to test the hypothesis that *Hs*ERp46 recruits a glycoprotein client to EDEM3 via mixed disulfide bonding, we tested trapping mutants of *Hs*ERp46 with *Hs*EDEM3 . We studied the *Hs*ERp46 *Hs*ERp46 C92A, C220A and C353A. The first and the last Cys residues correspond to *Ct*PDI C50 and C385 (they are located in the first and last TRX domains of *Hs*ERp46, respectively). The second one, C220A, traps disulfides to *Hs*ERp46 Cys217 of the *Hs*ERp46 extra redox motif ^{217}CXXC^{220}. This redox motif has no structural equivalent in *Ct*PDI as it is located in the middle TRX domain of *Hs*ERp46. In homology models of mammalian EDEM3:ERp46 complexes, this CXXC motif points away from the EDEM3:ERp46 interface.

Introduction of the Cys220Ala trapping mutant in *Hs*ERp46 resulted in loss of species corresponding to disulphide-bonded *Hs*EDEM3:*Hs*ERp46 heterodimer (Figure 8). In addition, the *Hs*EDEM3:*Hs*ERp46 heterodimer is present in two bands, likely corresponding to a redox equilibrium in which *Hs*EDEM3 C82-C441 intramolecular disulfide is either oxidised or reduced. The band for the reduced heterodimer is especially strong when species harbouring the C92A mutation are present. This suggests the *Hs*EDEM3 C82-C441 disulphide bond is mostly in a redox equilibrium with a disulfide involving *Hs*ERp46C89. This redox equilibrium is ablated by the C92A trapping mutant. Furthermore, this may suggest the main role of *Hs*ERp46 Cys350 is in forming an intermolecular disulphide bond with EDEM3.

Overall the data suggest that *Hs*ERp46 traps clients with a mixed disulfide at Cys217, and that upon formation of the covalent *Hs*EDEM3 Cys528:*Hs*ERp46 Cys350 SS-bonded heterodimer, reduction of a SS bond at *Hs*ERp46 C89 is in equilibrium with oxidation of *Hs*EDEM3 C82-C441. The redox equilibrium between the conserved intramolecular SS bond on the EDEM and a PDI disulfide is therefore crucial for the creation of a complex that possesses both mannosidase activity (EDEM in properly folded state, with its intramolecular bond oxidised) and ERAD reductase activity

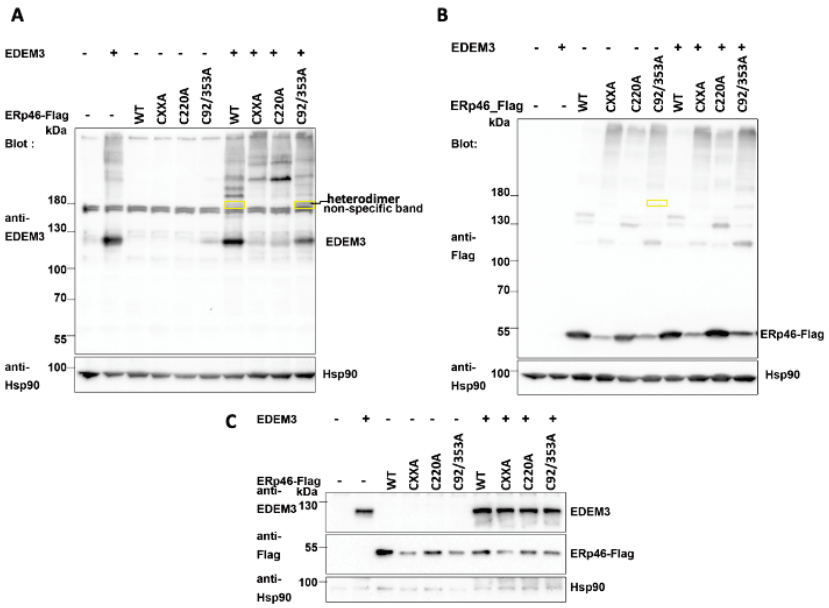

Fig. 8 The Cys220Ala *Hs*ERp46 trapping mutant favours the formation of SS-bonded ternary complexes *Hs*EDEM3-SS-*Hs*ERp46-SS-client. A.,B.,C. EDEM3 KO HEK293T cells co-transfected with *Hs*EDEM3 and *Hs*ERp46 WT and trapping mutants, as described in HEK293T transient transfection and Western blot analysis, were analysed by Western Blot in non-reducing (A., B.) and reducing conditions (C.). **A.** Detection of *Hs*EDEM3 and its covalently associated complexes, separated on a 6% polyacrylamide gel, transferred to a nitrocellulose membrane and detected with polyclonal anti-EDEM3 antibody; the yellow boxes indicate heterodimers and * a non-specific band. **B.** Detection of *Hs*ERp46 and its covalently associated complexes separated on a 6% polyacrylamide gel, transferred on a nitrocellulose membrane and detected with monoclonal anti-Flag HRP antibody. **C.** *Hs*EDEM3and *Hs*ERp46WT and trapping mutants were reduced, separated on an 8% polyacrylamide gel, transferred to a nitrocellulose membrane and detected with the same antibodies as in A. and B. Hsp90 was used as loading control in all the experiments.

(PDI has at least one reduced SS bond and reducing equivalents can be transferred to clients to aid their retrotranslocation).

Discussion

The ERAD checkpoint complex is essential for safeguarding eukaryotic cells against the accumulation of misfolded glycoproteins, which constitute about a third of the proteome [89]. Our study provides the most comprehensive structural and mechanistic insights to date into the function of the ERAD checkpoint complex, integrating cryo-EM structural studies, phylogenetic analyses, and biochemical data.

Cryo-EM structures of the ERAD checkpoint complex in both apo and ternary states (EDEM:PDI:A1AT-NHK) reveal two primary mechanisms for substrate recognition. The first involves recruitment of misfolded glycoproteins through solvent-exposed hydrophobic regions, aligning with prior observations that EDEM's flexible IMD-PAD

domain dynamically engages unfolded substrates. The second mechanism is mediated by reversible disulfide bonding between PDI and the substrate, allowing recognition of aberrant disulfide-linked multimers.

Phylogenetic and sequence analyses identify conserved disulfide-linked regulatory elements across eukaryotic EDEMs, from early eukaryotes to humans. The conserved intramolecular disulfide bond in the catalytic domain of all EDEMs, as well as unpaired cysteine residues at the C-terminal end of the catalytic domain, play critical roles in substrate processing. Notably, EDEM3 and its orthologues possess an additional unpaired cysteine that may further tighten EDEM:PDI interaction and/or be involved in redox chemistry and/or SSbond isomerism with clients.

Our findings also provide new insights into how the ERAD checkpoint selects glycoproteins for degradation. A short α-helix at the EDEM active site entry restricts access, ensuring specificity for mannose cleavage from Branch C, a key determinant in terminal misfolding signals. This specificity aligns with prior observations of glycan processing requirements in ERAD [58, 90]. However, glycan binding alone is not required for EDEM:PDI-mediated substrate recognition, as evidenced by interactions with NHK-A1AT even in the presence of kifunensine, which inhibits substrate binding. Instead, exposed hydrophobic surfaces and aberrant cysteine pairing likely serve as critical misfold recognition features.

Last but not least, published observations, re-interpreted in the light of our data, suggest that the EDEM GH47 domain is misfolded in isolation within the ER due to a reduced conserved intramolecular disulfide bond [19, 91]. Association with the PDI leads to an active EDEM:PDI complex, where the EDEM GH47 domain folds into a competent mannosidase while the PDI CXXC motif is reduced. This redox exchange enables EDEM to perform demannosylation—signaling terminal misfolding — while the PDI can function as an ERAD reductase, facilitating retro-translocation of misfolded glycoproteins [23, 25].

Beyond ERAD substrate processing in general, our findings have implications for protein misfolding disorders such as α1-antitrypsin deficiency (A1ATD) [7, 92]. The misfolded A1AT-Z variant, responsible for the most severe forms of A1ATD [93, 94], is primarily targeted by ERAD. Our structural data indicate that disrupting misfold interactions—either by modifying hydrophobic engagement or interfering with disulfide bond formation—could provide therapeutic strategies to mitigate the loss-of-function effects associated with A1ATD [95–98].

Together, our results clarify key mechanistic roles of the EDEM:PDI checkpoint complex in ERAD and set the foundation for targeting these interactions in protein misfolding diseases. By linking structural insights with functional validation, we provide a framework for future therapeutic strategies aimed at modulating ERAD activity in disease contexts.

Methods

Phylogeny

Sequence sets were constructed starting from the `AlphaFold Clusters` repository (https://cluster.foldseek.com/, [45]) in order to profit from the curation criteria used

to label the entries (including ≥50% identity and ≥90% overlap in sequence length) and from easy identification of the cluster members by UniProt IDs (*e.g. Homo sapiens* EDEM1:Q92611, EDEM2:Q9BV94, EDEM3:Q9BZQ6; *Arabidopsis thaliana* MNS4:Q9FG93, MNS5:Q9SXC9; *Chaetomium thermophilum* EDEM: G0SCX7).

The phylogenetic analysis was carried out with `IQ-TREE 2` [99] and the tree was visualized using the `ITOL Tree Server` [100].

Structure-based sequence alignment

Chaetomium thermophilum genes encoding ERAD checkpoint proteins were identified through a search of the *Ct* genome with the *Sc*HTM1P (Uniprot P38888) and *Sc*PDI1P (Uniprot P17967) sequences. The searches were carried out using the search tool on the server at https://c-thermophilum.bork.embl.de/. Top hits for the EDEM and PDI were used to search for orthologues using BlastP [101]. The AlphaFold models of the *Ct*EDEM and *Ct*PDI orthologues were downloaded from their Uniprot entry pages.

Structure-based sequence alignment of these sequences was carried out using Salign [47] and the resulting alignment was manually edited. Espript was used to illustrate sequence conservation [102]. The `ConSurf` server at []Yariv:2023ct was used to display sequence conservation on the structure.

Molecular cloning

The DNA sequence encoding Chaetomium thermophilum *Ct*EDEM (Uniprot G0SCX7) was obtained from GeneArt. *Ct*PDI DNA (Uniprot G0SGS2) was amplified from *Chaetomium thermophilum* cDNA (a gift of Ed Hurt, Biochemistry Centre, Heidelberg University, Heidelberg, Germany). Genes were amplified via PCR using Q5 High-Fidelity Polymerase. Vectors used were Litmus28i for cloning and pHLsec for mammalian expression. Litmus28i was linearized using EcoRI and XhoI, while pHLsec was linearized with AgeI and KpnI.

Primers with 5' overlaps tailored for Gibson assembly were designed. For *Ct*EDEM, a full-length codon-optimized gene was cloned into Litmus28i and pHLsec vectors. The N-terminal GFP fusion construct was generated by amplifying GFP and *Ct*EDEM fragments, followed by Gibson assembly into the pHLsec vector. The DNA sequence encoding for GFP protein was amplified using the plasmid pHLsec:GFP-SLC35B1 (Uniprot ID P78383), kindly donated by Dr Snežana Vasiljević (Biochemistry Department, University of Oxford). For *Ct*PDI, intron removal was achieved by amplifying the two exons separately, excluding the signal peptide and HDEL retrieval signal, and cloning them into pHLsec using Gibson assembly. Gibson assembly reactions were carried out with a 3:1 insert:vector molar ratio and incubated at 50°C for 1 hour. Site-directed mutagenesis of *Ct*PDI was carried out following a protocol outlined in [103]. DNA bands were verified via gel electrophoresis and purified when necessary using the GeneJet Gel Extraction Kit.

Competent DH5α *E. coli* cells were transformed with Gibson assembly products via heat shock and plated on LB agar containing carbenicillin (100 µg/mL). Colony-PCR was performed to confirm successful transformations. Plasmids were purified

using GeneJet Miniprep Kits for small-scale preparations and an adapted alkaline lysis protocol for large-scale maxipreps [104]. Purified plasmids were quantified via NanoDrop.

HEK293T transient transfection and Western blot analysis

EDEM3 knock-out HEK293T cells were cultured in DMEM supplemented with 10% FBS and transfected at 65–70% confluence using Polyethylenimine (PEI, 2.5:1 [v/w, PEI:DNA]). Cells were co-transfected with plasmids encoding A1AT-NHK:pCDNA3.1, *Ct*EDEM:pHLsec, *Ct*PDI:pHLsec, *Mm*EDEM3:pcDNA3.1, *Hs*ERp46:pcDNA3.1 controls, using optimized DNA ratios (e.g., 1:1:1 for *Ct*PDI:*Ct*EDEM:NHK triple expression or 3:1 for *Mm*EDEM3:*Hs*ERp46coexpression). For *Hs*ERp46trapping mutant experiments, cells were treated with 10 mM iodoacetamide prior to sampling.

Cells were lysed in Triton X-100 lysis buffer supplemented with protease inhibitors, phosphatase inhibitors, and 20 mM N-ethylmaleimide. Lysates were clarified by centrifugation at 14,000 × g for 20 minutes at 4°C, and protein concentrations were measured using the BCA assay. Equal protein amounts were separated by SDS-PAGE under reducing or non-reducing conditions (6–10% gels depending on the target) and transferred to 0.45 µm nitrocellulose membranes.

Membranes were blocked with 5% milk in TBS and incubated overnight at 4°C with primary antibodies (e.g., anti-A1AT, anti-His, anti-HA, anti-Flag, anti-EDEM3) diluted in 2.5% BSA in TBS. After washing, HRP-conjugated secondary antibodies were applied, and signals were detected using ECL substrate and a ChemiDoc Imaging system (Bio-Rad). Band intensities were quantified with ImageJ (v. 2.1.0) and normalized to the empty vector (EV) control. Statistical analyses were performed using one-way ANOVA with Dunnett's multiple comparisons test in GraphPad Prism v. 10.1.1. Error bars represent the standard deviation of three independent experiments.

Protein purification

Human embryonic kidney (HEK293F) cells were transfected using the method described in [105]. If multiple plasmids were co-transfected, equal amounts of each plasmid DNA was added.

The HEK293F cell culture was harvested 4 days post-transfection by centrifuging at 4,000 g for 5 minutes. The supernatant containing the secreted protein was adjusted to 1 x PBS pH 7.4 and filtered prior to IMAC. The filtered supernatant was passed onto a 1 mL HisTrap HP Ni IMAC column equilibrated against binding buffer (Na_2HPO_4 50 mM pH 7.5, NaCl 300 mM). The column was washed with 5 column volumes (CV) of wash buffer (Na_2HPO_4 50 mM pH 7.5, NaCl 300 mM, 10 mM imidazole). The proteins were eluted with a 15 CV gradient from 0% to 100% of elution buffer (Na_2HPO_4 50 mM pH 7.5, NaCl 200 mM, 500 mM imidazole.

The protein-containing fractions from IMAC were pooled and concentrated using a polyethersulfone (PES) membrane, 10 kDa MW cutoff centrifugal ultrafiltration device. This sample was then filtered through a 0.2 μm filter and applied to either a Superdex 200 Increase 10/300 GL/Superdex 200 16/600 pg (SEC) or Superdex 200 3.2/300 (microSEC) equilibrated against SEC buffer (HEPES 20 mM pH 7.5, NaCl 100

mM). SDS-PAGE of SEC fractions was used to assess purity (Thermo Fisher NuPAGE Bis-Tris 4-12% gel) and identify fractions of interest for downstream biochemical, structural, and proteomic studies.

Cryo-electron microscopy

Quantifoil Au300 R1.2/1.3 Holey Carbon grids were glow discharged using the EMS GloQube. For non-graphene oxidegrids, settings at 0.2 mBar, 35 mA for 60 seconds were used. For grids to be coated in graphene oxide, settings at 0.2 mBar, 50 mA for 75 seconds). Graphene oxide grid coating was carried out according to the protocol in [106]. Grids were blotted at blot force 10 for 3 seconds before plunge freezing immediately into liquid ethane using a Vitrobot Mark IV.

Cryo-EM data collection

Cryo-EM data collection was carried out on a FEI Titan Krios microscope with Gatan K3 detector at the Midlands Cryo-EM facility using the following settings: acceleration voltage was set to 300 kV; spherical aberration coefficient (Cs) was 2.7 mm; nominal magnification was 105,000x; calibrated pixel size was 0.835 Å; the second condenser aperture was set to 50 µm; the objective aperture was set to 100 µm; the defocus range was from -2.6 µm to -0.7 µm in 0.3 µm intervals; the detector was a K3 (Gatan, USA) in super resolution counting mode binned 2x; the energy filter slide width was 20 eV; the dose rate on the detector was measured over a typical specimen area and was 15 electrons/pixel/s; the dose rate on the specimen was measured over a hole and was 16.5 electrons/pixel/s; the exposure time was 3 sec/micrograph.

Cryo-EM data processing

Data processing was carried out in `RELION 4.0` [107] and cryoSPARC v4.1 [108], with the final *Ct*EDEM:*Ct*PDI reconstruction using cryoSPARC v4.1. In RELION, Motion correction used `MotionCor2` [109], CTF estimation used `CTFFind4` [110] and particle picking was carried out using `Topaz` [111] and autopicking software. In cryoSPARC, patch motion correction and patch CTF estimation were used, and particle used 2D templates from RELION for template picking. 2D classification was carried out in multiple rounds, each time removing particles that gave rise to poor quality classes. Ab-initio reconstruction was used to generate multiple initial 3D reconstructions. The various reconstructions were used alongside manufactured junk reconstructions to find and remove further junk particles. 3D classification was used to investigate structural heterogeneity within the dataset, and split particles into subsets. The subsets were refined using homogenous refinement and non-uniform refinement. Reconstructions were improved with local and global CTF refinements. Particle subtraction and local refinements were carried out by first generating masks against the regions of interest using `Create Mask` or `Volume Tools` in `UCSF Chimera` [112]. 3D variability analysis (3DVA) [113] was carried out using a consensus map from non-uniform refinement. 3DVA was run with 3 modes and filter resolution at 6Å. Output mode was set to simple with 20 components. The components of the three modes were visualized and recorded as movies in `Chimera` v1.9 using Volume Series.

Molecular Modelling

Homology models of *Chaetomium thermophilum* protein disulfide isomerase (*Ct*PDI) and ER-degradation enhancing alpha-like mannosidase protein (*Ct*EDEM) in complex were generated using `Alphafold-Multimer` [114]. Sequences were obtained from Uniprot (*Ct*PDI: [G0SGS2], residues 21–505; *Ct*EDEM: [G0SCX7], residues 64–1092) and processed with standard `Alphafold` parameters on the Midlands CryoEM facility computational cluster. Disordered regions with low confidence (local distance difference test score ≤ 75) were removed using a custom pruning script, yielding truncated models for docking into the EM map.

The cryo-EM density maps were generated in `cryoSPARC` and truncated `AlphaFold` maps were docked and refined with `Phenix` [115]. Models were rigid-body fitted with `Phenix.dock_in_map`, and real-space refinements were performed with `Phenix.real_space_refine` [116] using secondary structure and Ramachandran restraints. Missing loops were added iteratively with `Phenix.fit_loops` and manually built in `Coot` [117, 118] where required. Glycosylation sites were modeled using `Coot`'s carbohydrate module, followed by refinement in Phenix.

The `Coot` validation tools `Validate/Ramachandran Plot`, `Validate/Rotamer analysis` and `Validate/Validation Outliers` were used to improve errors in the structure. Favoured side chain rotamers were selected using the `Rotamers` tool. Real-space fit in `Coot` was carried out with Ramachandran restraints and the automated weight calculated by the program for the Cryo-EM map.

Plant biology

Plant material and growth conditions

Arabidopsis thaliana bri1-5 mutant and *mns4-1 mns5-1 bri1-5* triple mutant [41] were grown on soil at 22 °C and 70% relative humidity, under a 16-h-light/8-h-dark cycle (approximately 120 μmol m^{-2} s^{-1}).

Cloning of*Ct*EDEM:eGFP *Ct*EDEM:mRFP

The full-length coding sequence of *Ct*EDEM was amplified by PCR using the Accuprime Pfx DNA Polymerase (Invitrogen), cloned into pDONR™ 221 vector (Invitrogen) and sequenced. DNA primers used for cloning are "*Ct*EDEM_pDONR™ 221" in Table S1. Full-length *Ct*EDEM was then cloned using the Gateway® Technology into two destination vectors, pB7RWG2 and pK7WGF2

Binary vectors, containing the constructs, were amplified in *Escherichia coli* DH5α before transformation of *Agrobacterium tumefaciens* (strain GV3101).

Plant stable transformation

Later, the constructs *Ct*EDEM:mRFP and *Ct*EDEM:eGFP were used for stable transformation of the *Arabidopsis thaliana mns4-1/mns5-1/bri1-5* triple mutant. *Arabidopsis* plants were transformed using the floral dip method [119]. Healthy *Arabidopsis* plants were grown until they were flowering. *Agrobacterium tumefaciens* carrying gene *Ct*EDEM was spun down and resuspended to OD_{600}=0.8 in 500 mL of 5% Sucrose, 10

mM $MgCl_2$, 200 μM acetosyringone. Before dipping, Silwet L-77 was added to a concentration of 0.05% (500 μL/L). *At* was dipped in *Agrobacterium* solution for 1 minute and dipped plants were kept under a cover for 48 hours to maintain high humidity. After 5 days, the dipping procedure was repeated. Dry seeds were harvested and the transformants were selected on 1/2 MS medium with phosphinothricin (aka Basta, Duchefa P0159) for *Ct*EDEM:mRFP plants. With kanamycin for *Ct*EDEM:eGFP plants.

Confocal Laser Scanning Microscopy and *Ct*EDEM expression and localisation *in planta*

Confocal images were taken by a laser-scanning confocal microscope (LSM Pascal; Carl Zeiss). *Ct*EDEM:eGFP signal was excited at 488 nm with an argon laser and detected with a 505–530 nm filter set; whereas *Ct*EDEM:mRFP was excited at 543 nm with a He/Ne laser and detected in the 560–615 nm range. Chlorophyll autofluorescence was detected with the filter > 650 nm.

Declarations

Acknowledgements

We thank Radu Aricescu and Ed Hurt for donating the pHLsec vector and the *Ct* cDNA library, respectively. We acknowledge T.J. Ragan and the The Midlands Regional CryoEM Facility at the Leicester Institute of Structural and Chemical Biology (LISCB), major funding from MRC (MC_PC_17136).

Funding

C.J.H. was the recipient of an MRC IMPACT Programme Studentship and supported by the Membrane Protein Laboratory (funded by grant 223727/Z/21/Z from the Wellcome Trust) at the Diamond Light Source Ltd and Research Complex at Harwell. A.L. was the recipient of a PhD Studentship from the Agricultural and Forestry Department (DAFNE) of the University of Tuscia (Viterbo, Italy) and funding from the Italian National Research Council (to A.S.). P.R. was the recipient of an LISCB Wellcome Trust ISSF award, grant reference 204801/Z/16/Z and a Wellcome Trust Seed Award in Science, grant reference 214090/Z/18/Z. A.S. and P.R. were the recipients of a Research Project Prize 2021 (Grant code `Plant_EDEM` by the Department of Biological and Agro-alimentary Sciences of the Italian National Research Council). P.R. and S.P. were joint recipients of a bilateral grant from the Italian National Research Council and the Romanian Academy of Sciences.

Conflict of interest/Competing interests:

The authors declare no competing interests.

Data availability

Structure coordinates were deposited to the Research Collaboratory for Structural Bioinformatics PDB (https://www.rcsb.org/) and cryo-EM density maps used in model building were deposited to the EM Data Bank (https://www.ebi.ac.uk/pdbe/emdb) under the following accession codes: 8PKO and EMD-17749. Other data supporting the findings of this study are available from the corresponding authors on request.

Author contributions

P.R., A.S. and N.H. conceived and funded the study. P.R., A.T.C., A.L. and G.T. cloned the *Ct*EDEM and *Ct*PDI DNA constructs. P.R., G.T. and C.J.H. purified protein. C.J.H. prepared Cryo-EM grids. C.S. and C.J.H. collected Cryo-EM data. C.J.H and T.J.R. processed Cryo-EM data. P.R., Y.B. and C.J.H. built and refined the structural model. R.S., A.S. and M.d.B. carried out the experiments with *Ct*EDEM in plants. C.J.H, B.G, and A.Q carried out the A1AT-NHK ternary complex cryo-EM studies and *Ct*PDI trapping mutant studies. All authors contributed to the writing of the manuscript.

References

[1] Ermonval, M., Kitzmüller, C., Mir, A.M., Cacan, R., Ivessa, N.E.: N-glycan structure of a short-lived variant of ribophorin I expressed in the MadIA214 glycosylation-defective cell line reveals the role of a mannosidase that is not ER mannosidase I in the process of glycoprotein degradation. Glycobiology **11**(7), 565–576 (2001)

[2] Foulquier, F., Duvet, S., Klein, A., Mir, A.-M., Chirat, F., Cacan, R.: Endoplasmic reticulum-associated degradation of glycoproteins bearing Man5GlcNAc2 and Man9GlcNAc2 species in the MI8-5 CHO cell line. European journal of biochemistry **271**(2), 398–404 (2004)

[3] Helenius, A., Aebi, M.: Roles of n-linked glycans in the endoplasmic reticulum. Annual Review of Biochemistry **73**(1), 1019–1049 (2004) https://doi.org/10.1146/annurev.biochem.73.011303.073752 https://doi.org/10.1146/annurev.biochem.73.011303.073752. PMID: 15189166

[4] Vembar, S.S., Brodsky, J.L.: One step at a time: endoplasmic reticulum-associated degradation. Nature reviews. Molecular cell biology **9**(12), 944–957 (2008)

[5] Brodsky, J.: Cleaning up: Er-associated degradation to the rescue. Cell **151**(6), 1163–1167 (2012) https://doi.org/10.1016/j.cell.2012.11.012

[6] Sun, Z., Brodsky, J.L.: Protein quality control in the secretory pathway. The Journal of cell biology **218**(10), 3171–3187 (2019)

[7] Gooptu, B., Dickens, J.A., Lomas, D.A.: The molecular and cellular pathology of α1-antitrypsin deficiency. Trends in Molecular Medicine **20**(2), 116–127 (2014) https://doi.org/10.1016/j.molmed.2013.10.007

[8] Acosta-Alvear, D., Harnoss, J.M., Walter, P., Ashkenazi, A.: Homeostasis control in health and disease by the unfolded protein response. Nat Rev Mol Cell Biol (2024) https://doi.org/10.1038/s41580-024-00794-0

[9] Bigi, A., Lombardo, E., Cascella, R., Cecchi, C.: The toxicity of protein aggregates: New insights into the mechanisms. International Journal of Molecular Sciences **24**(9) (2023) https://doi.org/10.3390/ijms24097974

[10] Marciniak, S.J., Ron, D.: Endoplasmic reticulum stress signaling in disease. Physiological Reviews (2006) https://doi.org/10.1152/physrev.00015.2006.-The

[11] Bhattacharya, A., Qi, L.: ER-associated degradation in health and disease – from substrate to organism. Journal of Cell Science **132**(23) (2019)

[12] S, G., M, C., R, T., A, M.-V., SM, P.: Targeting edem protects against er stress

and improves development and survival in c. elegans. PLoS Genetics **18** (2022) https://doi.org/10.1371/journal.pgen.1010069

[13] Clerc, S., Hirsch, C., Oggier, D.M., Deprez, P., Jakob, C., Sommer, T., Aebi, M.: Htm1 protein generates the N-glycan signal for glycoprotein degradation in the endoplasmic reticulum. The Journal of cell biology **184**(1), 159–172 (2009)

[14] Hosokawa, N., Tremblay, L.O., Sleno, B., Kamiya, Y., Wada, I., Nagata, K., Kato, K., Herscovics, A.: EDEM1 accelerates the trimming of α1,2-linked mannose on the C branch of N-glycans. Glycobiology **20**(5), 567–575 (2010) https://doi.org/10.1093/glycob/cwq001 https://academic.oup.com/glycob/article-pdf/20/5/567/5845559/cwq001.pdf

[15] George, G., Ninagawa, S., Yagi, H., Saito, T., Ishikawa, T., Sakuma, T., Yamamoto, T., Imami, K., Ishihama, Y., Kato, K., Okada, T., Mori, K.: EDEM2 stably disulfide-bonded to TXNDC11 catalyzes the first mannose trimming step in mammalian glycoprotein ERAD. eLife **9** (2020)

[16] Zhang, J., Wu, J., Liu, L., Li, J.: The crucial role of demannosylating asparagine-linked glycans in eradicating misfolded glycoproteins in the endoplasmic reticulum. Frontiers in Plant Science **11** (2021) https://doi.org/10.3389/fpls.2020.625033 . Cited by: 6; All Open Access, Gold Open Access, Green Open Access

[17] Su, K., Stoller, T., Rocco, J., Zemsky, J., Green, R.: Pre-Golgi degradation of yeast prepro-alpha-factor expressed in a mammalian cell. Influence of cell type-specific oligosaccharide processing on intracellular fate. The Journal of biological chemistry **268**(19), 14301–14309 (1993)

[18] Pisoni, G.B., Molinari, M.: Five Questions (with their Answers) on ER-Associated Degradation. Traffic (Copenhagen, Denmark) **17**(4), 341–350 (2016)

[19] Sakoh-Nakatogawa, M., Nishikawa, S.-I., Endo, T.: Roles of protein-disulfide isomerase-mediated disulfide bond formation of yeast Mnl1p in endoplasmic reticulum-associated degradation. The Journal of biological chemistry **284**(18), 11815–11825 (2009)

[20] Liu, Y.-C., Fujimori, D.G., Weissman, J.S.: Htm1p–pdi1p is a folding-sensitive mannosidase that marks n-glycoproteins for er-associated protein degradation. Proceedings of the National Academy of Sciences **113**(28), 4015–4024 (2016) https://doi.org/10.1073/pnas.1608795113 https://www.pnas.org/content/113/28/E4015.full.pdf

[21] Gauss, R., Kanehara, K., Carvalho, P., Ng, D.T.W., Aebi, M.: A complex of Pdi1p and the mannosidase Htm1p initiates clearance of unfolded glycoproteins from the endoplasmic reticulum. Molecular Cell **42**(6), 782–793 (2011)

[22] Ushioda, R., Hoseki, J., Araki, K., Jansen, G., Thomas, D.Y., Nagata, K.: Erdj5 is required as a disulfide reductase for degradation of misfolded proteins in the er. Science **321**(5888), 569–572 (2008) https://doi.org/10.1126/science.1159293 https://science.sciencemag.org/content/321/5888/569.full.pdf

[23] Hagiwara, M., Maegawa, K.-I., Suzuki, M., Ushioda, R., Araki, K., Matsumoto, Y., Hoseki, J., Nagata, K., Inaba, K.: Structural basis of an ERAD pathway mediated by the ER-resident protein disulfide reductase ERdj5. Molecular cell **41**(4), 432–444 (2011)

[24] Timms, R.T., Menzies, S.A., Tchasovnikarova, I.A., Christensen, L.C., Williamson, J.C., Antrobus, R., Dougan, G., Ellgaard, L., Lehner, P.J.: Genetic dissection of mammalian erad through comparative haploid and crispr forward genetic screens. Nature Communications **7**(1), 11786 (2016) https://doi.org/10.1038/ncomms11786

[25] Maegawa, K.-i., Watanabe, S., Noi, K., Okumura, M., Amagai, Y., Inoue, M., Ushioda, R., Nagata, K., Ogura, T., Inaba, K.: The highly dynamic nature of erdj5 is key to efficient elimination of aberrant protein oligomers through er-associated degradation. Structure **25**(6), 846–8574 (2017) https://doi.org/10.1016/j.str.2017.04.001

[26] Lamriben, L., Oster, M.E., Tamura, T., Tian, W., Yang, Z., Clausen, H., Hebert, D.N.: Edem1's mannosidase-like domain binds erad client proteins in a redox-sensitive manner and possesses catalytic activity. J Biol Chem **293**(36), 13932–13945 (2018) https://doi.org/10.1074/jbc.RA118.004183

[27] Yu, S., Ito, S., Wada, I., Hosokawa, N.: Er-resident protein 46 (erp46) triggers the mannose-trimming activity of er degradation–enhancing α-mannosidase–like protein 3 (edem3). Journal of Biological Chemistry **293**(27), 10663–10674 (2018) https://doi.org/10.1074/jbc.RA118.003129

[28] Shenkman, M., Ron, E., Yehuda, R., Benyair, R., Khalaila, I., Lederkremer, G.Z.: Mannosidase activity of EDEM1 and EDEM2 depends on an unfolded state of their glycoprotein substrates. Communications biology **1**(1), 172 (2018)

[29] Manica, G., Ghenea, S., Munteanu, C.V.A., Martin, E.C., Butnaru, C., Surleac, M., Chiritoiu, G.N., Alexandru, P.R., Petrescu, A.-J., Petrescu, S.M.: Edem3 domains cooperate to perform its overall cell functioning. International Journal of Molecular Sciences **22**(4) (2021) https://doi.org/10.3390/ijms22042172

[30] Weng, S., Spiro, R.G.: Demonstration that a kifunensine-resistant alpha-mannosidase with a unique processing action on N-linked oligosaccharides occurs in rat liver endoplasmic reticulum and various cultured cells. Journal of Biological Chemistry **268**(34), 25656–25663 (1993)

[31] Hosokawa, N., Wada, I., Hasegawa, K., Yorihuzi, T., Tremblay, L.O., Herscovics, A., Nagata, K.: A novel ER alpha-mannosidase-like protein accelerates ER-associated degradation. EMBO reports **2**(5), 415–422 (2001)

[32] Olivari, S., Galli, C., Alanen, H., Ruddock, L., Molinari, M.: A novel stress-induced EDEM variant regulating endoplasmic reticulum-associated glycoprotein degradation. The Journal of biological chemistry **280**(4), 2424–2428 (2005)

[33] Hirao, K., Natsuka, Y., Tamura, T., Wada, I., Morito, D., Natsuka, S., Romero, P., Sleno, B., Tremblay, L.O., Herscovics, A., Nagata, K., Hosokawa, N.: EDEM3, a soluble EDEM homolog, enhances glycoprotein endoplasmic reticulum-associated degradation and mannose trimming. The Journal of biological chemistry **281**(14), 9650–9658 (2006)

[34] Ushioda, R., Hoseki, J., Nagata, K.: Glycosylation-independent erad pathway serves as a backup system under er stress. Mol Biol Cell **24**(20), 3155–3163 (2013) https://doi.org/10.1091/mbc.E13-03-0138

[35] Hebert, D.N., Molinari, M.: In and out of the ER: Protein folding, quality control, degradation, and related human diseases. Physiological Reviews **87**(4), 1377–1408 (2007) https://doi.org/10.1152/physrev.00050.2006

[36] Hebert, D.N., Lamriben, L., Powers, E.T., Kelly, J.W.: The intrinsic and extrinsic effects of N-linked glycans on glycoproteostasis. Nature Chemical Biology **10**(11), 902–910 (2014)

[37] Duwaerts, C.C., Maiers, J.L.: ER Disposal Pathways in Chronic Liver Disease: Protective, Pathogenic, and Potential Therapeutic Targets. Frontiers in molecular biosciences **8**, 804097 (2021)

[38] Quirke, J.C.K., Crich, D.: GH47 and Other Glycoside Hydrolases Catalyze Glycosidic Bond Cleavage with the Assistance of Substrate Super-arming at the Transition State. ACS catalysis **11**, 10308–10315 (2021)

[39] Sobala, Ł.F., Fernandes, P.Z., Hakki, Z., Thompson, A.J., Howe, J.D., Hill, M., Zitzmann, N., Davies, S., Stamataki, Z., Butters, T.D., Alonzi, D.S., Williams, S.J., Davies, G.J.: Structure of human endo-α-1,2-mannosidase (MANEA), an antiviral host-glycosylation target. Proceedings of the National Academy of Sciences of the United States of America **117**(47), 29595–29601 (2020)

[40] Lynch, M.: Gene duplication and evolution. In: Evolution From Molecules to Ecosystems. Oxford University Press, ??? (2004). https://doi.org/10.1093/oso/9780198515425.003.0004 . https://doi.org/10.1093/oso/9780198515425.003.0004

[41] Hüttner, S., Veit, C., Vavra, U., Schoberer, J., Liebminger, E., Maresch, D., Grass, J., Altmann, F., Mach, L., Strasser, R.: Arabidopsis class

i α-mannosidases MNS4 and MNS5 are involved in endoplasmic reticulum–associated degradation of misfolded glycoproteins. The Plant Cell **26**(4), 1712–1728 (2014) https://doi.org/10.1105/tpc.114.123216

[42] Ruddock, L.W., Molinari, M.: N-glycan processing in er quality control. J Cell Sci **119**(Pt 21), 4373–4380 (2006) https://doi.org/10.1242/jcs.03225

[43] Balaji, S., Srinivasan, N.: Comparison of sequence-based and structure-based phylogenetic trees of homologous proteins: Inferences on protein evolution. Journal of Biosciences **32**(1), 83–96 (2007) https://doi.org/10.1007/s12038-007-0008-1

[44] Malik, A.J., Poole, A.M., Allison, J.R.: Structural phylogenetics with confidence. Molecular Biology and Evolution **37**(9), 2711–2726 (2020) https://doi.org/10.1093/molbev/msaa100 https://academic.oup.com/mbe/article-pdf/37/9/2711/33866729/msaa100.pdf

[45] Kempen, M., Kim, S.S., Tumescheit, C., Mirdita, M., Lee, J., Gilchrist, C.L.M., Söding, J., Steinegger, M.: Fast and accurate protein structure search with foldseek. Nature Biotechnology **42**(2), 243–246 (2024) https://doi.org/10.1038/s41587-023-01773-0

[46] Krogh, A., Larsson, B., von Heijne, G., Sonnhammer, E.L.L.: Predicting transmembrane protein topology with a hidden markov model: application to complete genomes11edited by f. cohen. Journal of Molecular Biology **305**(3), 567–580 (2001) https://doi.org/10.1006/jmbi.2000.4315

[47] Ayub, U., Haider, I., Naveed, H.: SAlign–a structure aware method for global PPI network alignment. BMC Bioinformatics **21**(1), 500 (2020)

[48] Jumper, J., Evans, R., Pritzel, A., Green, T., Figurnov, M., Ronneberger, O., Tunyasuvunakool, K., Bates, R., Žídek, A., Potapenko, A., Bridgland, A., Meyer, C., Kohl, S.A.A., Ballard, A.J., Cowie, A., Romera-Paredes, B., Nikolov, S., Jain, R., Adler, J., Back, T., Petersen, S., Reiman, D., Clancy, E., Zielinski, M., Steinegger, M., Pacholska, M., Berghammer, T., Silver, D., Vinyals, O., Senior, A.W., Kavukcuoglu, K., Kohli, P., Hassabis, D.: Applying and improving AlphaFold at CASP14. Proteins **89**(12), 1711–1721 (2021)

[49] Zhao, D., Wu, X., Rapoport, T.A.: Initiation of erad by the bifunctional complex of mnl1 mannosidase and protein disulfide isomerase. bioRxiv (2024) https://doi.org/10.1101/2024.10.17.618908 https://www.biorxiv.org/content/early/2024/10/17/2024.10.17.618908.full.pdf

[50] Leuenberger, P., Ganscha, S., Kahraman, A., Cappelletti, V., Boersema, P.J., Mering, C., Claassen, M., Picotti, P.: Cell-wide analysis of protein thermal unfolding reveals determinants of thermostability. Science **355**(6327), 7825 (2017) https://doi.org/10.1126/science.aai7825

https://www.science.org/doi/pdf/10.1126/science.aai7825

[51] Hüttner, S., Veit, C., Schoberer, J., Grass, J., Strasser, R.: Unraveling the function of arabidopsis thaliana OS9 in the endoplasmic reticulum-associated degradation of glycoproteins. Plant Molecular Biology **79**(1-2), 21–33 (2012) https://doi.org/10.1007/s11103-012-9891-4

[52] Ronzoni, R., Berardelli, R., Medicina, D., Sitia, R., Gooptu, B., Fra, A.M.: Aberrant disulphide bonding contributes to the er retention of alpha1-antitrypsin deficiency variants. Human Molecular Genetics **25**(4), 642–650 (2015) https://doi.org/10.1093/hmg/ddv501 https://academic.oup.com/hmg/article-pdf/25/4/642/18526797/ddv501.pdf

[53] Vagin, A., Teplyakov, A.: Molecular replacement with MOLREP. Acta crystallographica. Section D, Biological crystallography **66**(Pt 1), 22–25 (2010)

[54] Alexander, L.T., Durairaj, J., Kryshtafovych, A., Abriata, L.A., Bayo, Y., Bhabha, G., Breyton, C., Caulton, S.G., Chen, J., Degroux, S., Ekiert, D.C., Erlandsen, B.S., Freddolino, P.L., Gilzer, D., Greening, C., Grimes, J.M., Grinter, R., Gurusaran, M., Hartmann, M.D., Hitchman, C.J., Keown, J.R., Kropp, A., Kursula, P., Lovering, A.L., Lemaitre, B., Lia, A., Liu, S., Logotheti, M., Lu, S., Markússon, S., Miller, M.D., Minasov, G., Niemann, H.H., Opazo, F., Phillips, G.N.J., Davies, O.R., Rommelaere, S., Rosas-Lemus, M., Roversi, P., Satchell, K., Smith, N., Wilson, M.A., Wu, K.-L., Xia, X., Xiao, H., Zhang, W., Zhou, Z.H., Fidelis, K., Topf, M., Moult, J., Schwede, T.: Protein target highlights in casp15: Analysis of models by structure providers. Proteins **91**(12), 1571–1599 (2023) https://doi.org/10.1002/prot.26545

[55] Vallée, F., Karaveg, K., Herscovics, A., Moremen, K.W., Howell, P.L.: Structural basis for catalysis and inhibition of N-glycan processing class I alpha 1,2-mannosidases. Journal of Biological Chemistry **275**(52), 41287–41298 (2000)

[56] Vallée, F., Lipari, F., Yip, P., Sleno, B., Herscovics, A., Howell, P.L.: Crystal structure of a class I alpha1,2-mannosidase involved in N-glycan processing and endoplasmic reticulum quality control. The EMBO Journal **19**(4), 581–588 (2000)

[57] Olivari, S., Cali, T., Salo, K.E.H., Paganetti, P., Ruddock, L.W., Molinari, M.: EDEM1 regulates ER-associated degradation by accelerating de-mannosylation of folding-defective polypeptides and by inhibiting their covalent aggregation. Biochemical and Biophysical Research Communications **349**(4), 1278–1284 (2006) https://doi.org/10.1016/j.bbrc.2006.08.186

[58] Ninagawa, S., Okada, T., Sumitomo, Y., Kamiya, Y., Kato, K., Horimoto, S., Ishikawa, T., Takeda, S., Sakuma, T., Yamamoto, T., Mori, K.: EDEM2 initiates mammalian glycoprotein ERAD by catalyzing the first mannose trimming step. The Journal of cell biology **206**(3), 347–356 (2014)

[59] Xiang, Y., Karaveg, K., Moremen, K.W.: Substrate recognition and catalysis by GH47 α-mannosidases involved in Asn-linked glycan maturation in the mammalian secretory pathway. Proceedings of the National Academy of Sciences of the United States of America **113**(49), 7890–7899 (2016)

[60] Holm, L., Rosenström, P.: Dali server: conservation mapping in 3D. Nucleic acids research **38**(Web Server issue), 545–9 (2010)

[61] Pfeiffer, A., Stephanowitz, H., Krause, E., Volkwein, C., Hirsch, C., Jarosch, E., Sommer, T.: A Complex of Htm1 and the Oxidoreductase Pdi1 Accelerates Degradation of Misfolded Glycoproteins. The Journal of biological chemistry **291**(23), 12195–12207 (2016)

[62] Molinari, M.: Role of EDEM in the release of misfolded glycoproteins from the calnexin cycle. Science **299**(5611), 1397–1400 (2003) https://doi.org/10.1126/science.1079474

[63] Oda, Y., Hosokawa, N., Wada, I., Nagata, K.: EDEM as an acceptor of terminally misfolded glycoproteins released from calnexin. Science (New York, N.Y.) **299**(5611), 1394–1397 (2003)

[64] Mast, S.W., Diekman, K., Karaveg, K., Davis, A., Sifers, R.N., Moremen, K.W.: Human EDEM2, a novel homolog of family 47 glycosidases, is involved in ER-associated degradation of glycoproteins. Glycobiology **15**(4), 421–436 (2005)

[65] Tempel, W., Karaveg, K., Liu, Z.-J., Rose, J., Wang, B.-C., Moremen, K.W.: Structure of mouse golgi α-mannosidase ia reveals the molecular basis for substrate specificity among class 1 (family 47 glycosylhydrolase) α1,2-mannosidases*. Journal of Biological Chemistry **279**(28), 29774–29786 (2004) https://doi.org/10.1074/jbc.M403065200

[66] Bedem, H., Wilson, M.A.: Shining light on cysteine modification: connecting protein conformational dynamics to catalysis and regulation. Journal of Synchrotron Radiation **26**(4), 958–966 (2019) https://doi.org/10.1107/S160057751900568X

[67] Tempel, W., Karaveg, K., Liu, Z.-J., Rose, J., Wang, B.-C., Moremen, K.W.: Structure of mouse golgiα-mannosidase ia reveals the molecular basis for substrate specificity among class 1 (family 47 glycosylhydrolase) 1,2-mannosidases*. Journal of Biological Chemistry **279**(28), 29774–29786 (2004) https://doi.org/10.1074/jbc.M403065200

[68] Chinnaraj, M., Flaumenhaft, R., Pozzi, N.: Reduction of protein disulfide isomerase results in open conformations and stimulates dynamic exchange between structural ensembles. Journal of Biological Chemistry **298**(8), 102217 (2022) https://doi.org/10.1016/J.JBC.2022.102217

[69] Yagi-Utsumi, M., Miura, H., Ganser, C., Watanabe, H., Hiranyakorn, M., Satoh,

T., Uchihashi, T., Kato, K., Okazaki, K.-i., Aoki, K.: Molecular design of fret probes based on domain rearrangement of protein disulfide isomerase for monitoring intracellular redox status. International Journal of Molecular Sciences **24**(16) (2023) https://doi.org/10.3390/ijms241612865

[70] Lyles, M.M., Gilbert, H.F.: Mutations in the thioredoxin sites of protein disulfide isomerase reveal functional nonequivalence of the n- and c-terminal domains. J Biol Chem **269**(49), 30946–30952 (1994)

[71] Pandhare, J., Deshpande, V.: Both chaperone and isomerase functions of protein disulfide isomerase are essential for acceleration of the oxidative refolding and reactivation of dimeric alkaline protease inhibitor. Protein Sci **13**(9), 2493–2501 (2004) https://doi.org/10.1110/ps.03552004

[72] Sokołowska, I., Piłka, E.S., Sandvig, K., Wegrzyn, G., Slomińska-Wojewódzka, M.: Hydrophobicity of protein determinants influences the recognition of substrates by EDEM1 and EDEM2 in human cells. BMC Cell Biology **16**(1), 1–18 (2015) https://doi.org/10.1186/s12860-015-0047-7

[73] Georgescauld, F., Popova, K., Gupta, A.J., Bracher, A., Engen, J.R., Hayer-Hartl, M., Hartl, F.U.: Groel/es chaperonin modulates the mechanism and accelerates the rate of tim-barrel domain folding. Cell **157**, 922–934 (2014) https://doi.org/10.1016/j.cell.2014.03.038

[74] Pobre, K.F.R., Poet, G.J., Hendershot, L.M.: The endoplasmic reticulum (er) chaperone bip is a master regulator of er functions: Getting by with a little help from erdj friends. Journal of Biological Chemistry **294**, 2098–2108 (2019) https://doi.org/10.1074/jbc.REV118.002804

[75] Ninagawa, S., Matsuo, M., Ying, D., Oshita, S., Aso, S., Matsushita, K., Taniguchi, M., Fueki, A., Yamashiro, M., Sugasawa, K., Saito, S., Imami, K., Kizuka, Y., Sakuma, T., Yamamoto, T., Yagi, H., Kato, K., Mori, K.: Uggt1-mediated reglucosylation of n-glycan competes with er-associated degradation of unstable and misfolded glycoproteins. Elife **12** (2024) https://doi.org/10.7554/eLife.93117

[76] Wang, N., Seko, A., Takeda, Y., Ito, Y.: Glycan dependent refolding activity of er glucosyltransferase (uggt). Biochim Biophys Acta Gen Subj **1864**(12), 129709 (2020) https://doi.org/10.1016/j.bbagen.2020.129709

[77] Modenutti, C.P., Capurro, J.I.B., Ibba, R., Alonzi, D.S., Song, M.N., Vasiljević, S., Kumar, A., Chandran, A.V., Tax, G., Marti, L., Hill, J.C., Lia, A., Hensen, M., Waksman, T., Rushton, J., Rubichi, S., Santino, A., Martí, M.A., Zitzmann, N., Roversi, P.: Clamping, bending, and twisting inter-domain motions in the misfold-recognizing portion of udp-glucose: Glycoprotein glucosyltransferase. Structure **29**, 357–3709 (2021) https://doi.org/10.1016/j.str.2020.11.017

[78] Williams, R.V., Guay, K.P., Hurlbut Lesk, O.A., Clerico, E.M., Hebert, D.N., Gierasch, L.M.: Insights into the interaction between uggt, the gatekeeper of folding in the er, and its partner, the selenoprotein sep15. Proc Natl Acad Sci U S A **121**(34), 2315009121 (2024) https://doi.org/10.1073/pnas.2315009121

[79] Taylor, S.C., Thibault, P., Tessier, D.C., Bergeron, J.J.M., Thomas, D.Y.: Glycopeptide specificity of the secretory protein folding sensor udp-glucose glycoprotein:glucosyltransferase. EMBO Rep **4**(4), 405–411 (2003) https://doi.org/10.1038/sj.embor.embor797

[80] Izumi, M., Kuruma, R., Okamoto, R., Seko, A., Ito, Y., Kajihara, Y.: Substrate recognition of glycoprotein folding sensor uggt analyzed by site-specifically 15n-labeled glycopeptide and small glycopeptide library prepared by parallel native chemical ligation. Journal of the American Chemical Society **139**(33), 11421–11426 (2017) https://doi.org/10.1021/jacs.7b03277

[81] Hebditch, M., Warwicker, J.: Web-based display of protein surface and pH-dependent properties for assessing the developability of biotherapeutics. Scientific Reports **9**(1), 1–9 (2019) https://doi.org/10.1038/s41598-018-36950-8

[82] Meng, E.C., Goddard, T.D., Pettersen, E.F., Couch, G.S., Pearson, Z.J., Morris, J.H., Ferrin, T.E.: Ucsf chimerax: Tools for structure building and analysis. Protein Science **32**(11), 4792 (2023) https://doi.org/10.1002/pro.4792 https://onlinelibrary.wiley.com/doi/pdf/10.1002/pro.4792

[83] Kozlov, G., Määttänen, P., Thomas, D.Y., Gehring, K.: A structural overview of the PDI family of proteins. FEBS Journal **277**(19), 3924–3936 (2010) https://doi.org/10.1111/j.1742-4658.2010.07793.x

[84] Molinari, M., Galli, C., Piccaluga, V., Pieren, M., Paganetti, P.: Sequential assistance of molecular chaperones and transient formation of covalent complexes during protein degradation from the ER. The Journal of cell biology **158**(2), 247–257 (2002)

[85] Jessop, C.E., Chakravarthi, S., Garbi, N., Hämmerling, G.J., Lovell, S., Bulleid, N.J.: Erp57 is essential for efficient folding of glycoproteins sharing common structural domains. The EMBO Journal **26**(1), 28–40 (2007) https://doi.org/10.1038/sj.emboj.7601505 https://www.embopress.org/doi/pdf/10.1038/sj.emboj.7601505

[86] Kojima, R., Okumura, M., Masui, S., Kanemura, S., Inoue, M., Saiki, M., Yamaguchi, H., Hikima, T., Suzuki, M., Akiyama, S., Inaba, K.: Radically Different Thioredoxin Domain Arrangement of ERp46, an Efficient Disulfide Bond Introducer of the Mammalian PDI Family. Structure/Folding and Design **22**(3), 431–443 (2014)

[87] Su, C.-C., Lyu, M., Zhang, Z., Miyagi, M., Huang, W., Taylor, D.J., Yu, E.W.:

High-resolution structural-omics of human liver enzymes. Cell reports **42**(6) (2023)

[88] Jessop, C.E., Watkins, R.H., Simmons, J.J., Tasab, M., Bulleid, N.J.: Protein disulphide isomerase family members show distinct substrate specificity: P5 is targeted to BiP client proteins. Journal of cell science **122**(Pt 23), 4287–4295 (2009)

[89] Juszkiewicz, S., Hegde, R.S.: Quality control of orphaned proteins. Molecular Cell **71**, 443–457 (2018) https://doi.org/10.1016/j.molcel.2018.07.001 . doi: 10.1016/j.molcel.2018.07.001

[90] George, G., Ninagawa, S., Yagi, H., Furukawa, J.-i., Hashii, N., Ishii-Watabe, A., Deng, Y., Matsushita, K., Ishikawa, T., Mamahit, Y.P., Maki, Y., Kajihara, Y., Kato, K., Okada, T., Mori, K.: Purified edem3 or edem1 alone produces determinant oligosaccharide structures from m8b in mammalian glycoprotein erad. eLife **10**, 70357 (2021) https://doi.org/10.7554/eLife.70357

[91] Lipari, F., Herscovics, A.: Role of the cysteine residues in the alpha1,2-mannosidase involved in n-glycan biosynthesis in saccharomyces cerevisiae. the conserved cys340 and cys385 residues form an essential disulfide bond. J Biol Chem **271**(44), 27615–27622 (1996) https://doi.org/10.1074/jbc.271.44.27615

[92] Gooptu, B.: Surfactant protein c mutations and familial pulmonary fibrosis: stuck in a loop on the scenic route. European Respiratory Journal **59**(1) (2022) https://doi.org/10.1183/13993003.02147-2021 https://publications.ersnet.org//content/erj/59/1/2102147.full.pdf

[93] Nakanishi, T., Forgetta, V., Handa, T., Hirai, T., Mooser, V., Lathrop, G.M., Cookson, W.O.C.M., Richards, J.B.: The undiagnosed disease burden associated with alpha-1 antitrypsin deficiency genotypes. European Respiratory Journal **56**(6) (2020) https://doi.org/10.1183/13993003.01441-2020 https://publications.ersnet.org//content/erj/56/6/2001441.full.pdf

[94] Fromme, M., Schneider, C.V., Pereira, V., Hamesch, K., Pons, M., Reichert, M.C., Benini, F., Ellis, P., H Thorhauge, K., Mandorfer, M., Burbaum, B., Woditsch, V., Chorostowska-Wynimko, J., Verbeek, J., Nevens, F., Genesca, J., Miravitlles, M., Nuñez, A., Schaefer, B., Zoller, H., Janciauskiene, S., Abreu, N., Jasmins, L., Gaspar, R., Liberal, R., Macedo, G., Mahadeva, R., Gomes, C., Schneider, K.M., Trauner, M., Krag, A., Gooptu, B., Thorburn, D., Marshall, A., Hurst, J.R., Lomas, D.A., Lammert, F., Gaisa, N.T., Clark, V., Griffiths, W., Trautwein, C., Turner, A.M., McElvaney, N.G., Strnad, P.: Hepatobiliary phenotypes of adults with alpha-1 antitrypsin deficiency. Gut **71**(2), 415–423 (2022) https://doi.org/10.1136/gutjnl-2020-323729 https://gut.bmj.com/content/71/2/415.full.pdf

[95] Le, A., Ferrell, G.A., Dishon, D.S., Le, Q.Q.A., Sifers, R.N.: Soluble aggregates

of the human piz 1-antitrypsin variant are degraded within the endoplasmic reticulum by a mechanism sensitive to inhibitors of protein synthesis. Journal of Biological Chemistry **267**, 1072–1080 (1992) https://doi.org/10.1016/s0021-9258(18)48397-4

[96] Cabral, C.M., Liu, Y., Moremen, K.W., Sifers, R.N.: Organizational diversity among distinct glycoprotein endoplasmic reticulum-associated degradation programs. Molecular Biology of the Cell **13**(8), 2639–2650 (2002) https://doi.org/10.1091/mbc.e02-02-0068 https://doi.org/10.1091/mbc.e02-02-0068. PMID: 12181335

[97] Kroeger, H., Miranda, E., MacLeod, I., Pérez, J., Crowther, D.C., Marciniak, S.J., Lomas, D.A.: Endoplasmic reticulum-associated degradation (erad) and autophagy cooperate to degrade polymerogenic mutant serpins *. Journal of Biological Chemistry **284**, 22793–22802 (2009) https://doi.org/10.1074/jbc.M109.027102 . doi: 10.1074/jbc.M109.027102

[98] Bouchecareilh, M., Hutt, D.M., Szajner, P., Flotte, T.R., Balch, W.E.: Histone deacetylase inhibitor (hdaci) suberoylanilide hydroxamic acid (saha)-mediated correction of 1-antitrypsin deficiency *. Journal of Biological Chemistry **287**, 38265–38278 (2012) https://doi.org/10.1074/jbc.M112.404707 . doi: 10.1074/jbc.M112.404707

[99] Minh, B.Q., Schmidt, H.A., Chernomor, O., Schrempf, D., Woodhams, M.D., Haeseler, A., Lanfear, R.: Iq-tree 2: New models and efficient methods for phylogenetic inference in the genomic era. Mol Biol Evol **37**(5), 1530–1534 (2020) https://doi.org/10.1093/molbev/msaa015

[100] Letunic, I., Bork, P.: Interactive tree of life (itol) v6: recent updates to the phylogenetic tree display and annotation tool. Nucleic Acids Res **52**(W1), 78–82 (2024) https://doi.org/10.1093/nar/gkae268

[101] Altschul, S.F., Gish, W., Miller, W., Myers, E.W., Lipman, D.J.: Basic local alignment search tool. Journal of Molecular Biology **215**(3), 403–410 (1990) https://doi.org/10.1016/S0022-2836(05)80360-2

[102] Robert, X., Gouet, P.: Deciphering key features in protein structures with the new ENDscript server. Nucleic Acids Research **42**(W1), 320–324 (2014) https://doi.org/10.1093/nar/gku316 https://academic.oup.com/nar/article-pdf/42/W1/W320/17422987/gku316.pdf

[103] Heckman, K.L., Pease, L.R.: Gene splicing and mutagenesis by pcr-driven overlap extension. Nature Protocols **2**, 924–932 (2007) https://doi.org/10.1038/nprot.2007.132

[104] Feliciello, I., Chinali, G.: A modified alkaline lysis method for the preparation of highly purified plasmid dna from escherichia coli. Analytical Biochemistry

212(2), 394–401 (1993) https://doi.org/10.1006/abio.1993.1346

[105] Portolano, N., Watson, P.J., Fairall, L., Millard, C.J., Milano, C.P., Song, Y., Cowley, S.M., Schwabe, J.W.R.: Recombinant protein expression for structural biology in HEK 293f suspension cells: A novel and accessible approach. Journal of Visualized Experiments (92) (2014) https://doi.org/10.3791/51897

[106] Bokori-Brown, M., Martin, T.G., Naylor, C.E., Basak, A.K., Titball, R.W., Savva, C.G.: Cryo-em structure of lysenin pore elucidates membrane insertion by an aerolysin family protein. Nature Communications **7** (2016) https://doi.org/10.1038/ncomms11293

[107] Kimanius, D., Dong, L., Sharov, G., Nakane, T., Scheres, S.H.W.: New tools for automated cryo-EM single-particle analysis in RELION-4.0. Biochemical Journal **478**(24), 4169–4185 (2021) https://doi.org/10.1042/BCJ20210708

[108] Punjani, A., Rubinstein, J.L., Fleet, D.J., Brubaker, M.A.: Cryosparc: Algorithms for rapid unsupervised cryo-em structure determination. Nature Methods **14**, 290–296 (2017) https://doi.org/10.1038/nmeth.4169

[109] Zheng, S., Palovcak, E., Armache, J.-P., Cheng, Y., Agard, D.: Anisotropic Correction of Beam-induced Motion for Improved Single-particle Electron Cryo-microscopy. bioRxiv, 1–30 (2016)

[110] Rohou, A., Grigorieff, N.: CTFFIND4: Fast and accurate defocus estimation from electron micrographs. Journal of Structural Biology **192**(2), 216–221 (2015) https://doi.org/10.1016/j.jsb.2015.08.008

[111] Bepler, T., Kelley, K., Noble, A.J., Berger, B.: Topaz-Denoise: general deep denoising models for cryoEM and cryoET. Nature Communications **11**(1) (2020) https://doi.org/10.1038/s41467-020-18952-1

[112] Goddard, T.D., Huang, C.C., Meng, E.C., Pettersen, E.F., Couch, G.S., Morris, J.H., Ferrin, T.E.: UCSF ChimeraX: Meeting modern challenges in visualization and analysis. Protein Science **27**(1), 14–25 (2018) https://doi.org/10.1002/pro.3235

[113] Punjani, A., Fleet, D.J.: 3D variability analysis: Resolving continuous flexibility and discrete heterogeneity from single particle cryo-EM. Journal of Structural Biology **213**(2), 107702 (2021) https://doi.org/10.1016/j.jsb.2021.107702

[114] Evans, R., O'neill, M., Pritzel, A., Antropova, N., Senior, A., Green, T., Žídek, A., Bates, R., Blackwell, S., Yim, J., Ronneberger, O., Bodenstein, S., Zielinski, M., Bridgland, A., Potapenko, A., Cowie, A., Tunyasuvunakool, K., Jain, R., Clancy, E., Kohli, P., Jumper, J., Hassabis, D.: Protein complex prediction with alphafold-multimer. bioRxiv (2022) https://doi.org/10.1101/2021.10.04.463034

[115] Liebschner, D., Afonine, P.V., Baker, M.L., Bunkoczi, G., Chen, V.B., Croll, T.I., Hintze, B., Hung, L.W., Jain, S., McCoy, A.J., Moriarty, N.W., Oeffner, R.D., Poon, B.K., Prisant, M.G., Read, R.J., Richardson, J.S., Richardson, D.C., Sammito, M.D., Sobolev, O.V., Stockwell, D.H., Terwilliger, T.C., Urzhumtsev, A.G., Videau, L.L., Williams, C.J., Adams, P.D.: Macromolecular structure determination using X-rays, neutrons and electrons: Recent developments in Phenix. Acta Crystallographica Section D: Structural Biology **75**, 861–877 (2019) https://doi.org/10.1107/S2059798319011471

[116] Afonine, P.V., Poon, B.K., Read, R.J., Sobolev, O.V., Terwilliger, T.C., Urzhumtsev, A., Adams, P.D.: Real-space refinement in PHENIX for cryo-EM and crystallography. urn:issn:2059-7983 **74**(6), 531–544 (2018) https://doi.org/10.1107/S2059798318006551

[117] Emsley, P., Cowtan, K.: Coot: Model-building tools for molecular graphics. Acta Crystallographica Section D: Biological Crystallography **60**(12 I), 2126–2132 (2004) https://doi.org/10.1107/S0907444904019158

[118] Casañal, A., Lohkamp, B., Emsley, P.: Current developments in Coot for macromolecular model building of Electron Cryo-microscopy and Crystallographic Data. Protein Science **29**(4), 1069–1078 (2020) https://doi.org/10.1002/pro.3791

[119] Clough, S.J., Bent, A.F.: Floral dip: a simplified method forAgrobacterium-mediated transformation ofArabidopsis thaliana. The Plant Journal **16**(6), 735–743 (1998) https://doi.org/10.1046/j.1365-313x.1998.00343.x

[120] McNicholas, S., Agirre, J.: Glycoblocks: a schematic three-dimensional representation for glycans and their interactions. Acta crystallographica. Section D, Structural biology **73**(Pt 2), 187–194 (2017)